

Generative modeling with Gaussian Boson Sampling: classically trainable Bosonic Born Machines

Zoltán Kolarovszki^{1,2}, Bence Bakó^{1,2}, Michał Oszmaniec³, Changhun Oh⁴, and
Zoltán Zimborás^{1,5,6}

¹HUN-REN Wigner Research Centre for Physics, Budapest, Hungary

²Eötvös Loránd University, Budapest, Hungary

³Center for Quantum Enabled-Computing, Center for Theoretical Physics of
the Polish Academy of Sciences, Al. Lotników 32/46, 02-668 Warsaw, Poland

⁴Department of Physics, Korea Advanced Institute of Science and Technology,
Daejeon 34141, Korea

⁵University of Helsinki, Yliopistonkatu 4 00100 Helsinki, Finland

⁶Algorithmiq Ltd, Kanavakatu 3C 00160 Helsinki, Finland

Abstract

Quantum generative modeling has emerged as a promising application of quantum computers, aiming to model complex probability distributions beyond the reach of classical methods. In practice, however, training such models often requires costly gradient estimation performed directly on the quantum hardware. Crucially, for certain structured quantum circuits, expectation values of local observables can be efficiently evaluated on a classical computer, enabling classical training without calls to the quantum hardware in the optimization loop. In these models, sampling from the resulting circuits can still be classically hard, so inference must be performed on a quantum device, yielding a potential computational advantage. In this work, we introduce a photonic quantum generative model built on parametrized Gaussian Boson Sampling circuits. The training is based on the efficient classical evaluation of expectation values enabled by the Gaussian structure of the state, allowing scalable optimization of the model parameters through the maximum mean discrepancy loss function. We demonstrate the effectiveness of the approach through numerical experiments on photonic systems with up to 805 modes and over a million trainable parameters, highlighting its scalability and suitability for near-term photonic quantum devices.

1 Introduction

The success of classical deep learning is closely linked to the favorable trainability of deep neural networks, enabled by efficient gradient computation techniques that support optimization in high-dimensional parameter spaces [1–3]. In contrast, quantum machine learning (QML) models face many challenges, including unfavorable loss landscape [4–6], lack of automatic differentiation via backpropagation [7, 8] and significant shot-noise in loss function evaluations [9]. More concretely, unlike classical neural networks, where gradients can often be computed at a cost comparable to loss evaluation, standard gradient-estimation techniques for parametrized quantum circuits require a number of circuit evaluations that scales with the number of trainable parameters [10–13]. For large models, this leads to a substantial sampling overhead, which is further exacerbated by the comparatively low sampling rates of current quantum hardware [9], the inherently probabilistic nature of quantum measurements, and barren plateaus [5, 6].

Proposed strategies for overcoming such challenges include developing more efficient gradient estimation methods [14–16] and restricting circuit architectures to improve loss landscapes [17–21]. However, the conditions that ensure good trainability in quantum models by avoiding barren plateaus often align with the ability to efficiently simulate expectation values of local observables using classical methods. This presents a challenge for supervised quantum machine learning models, as they typically output such expectation values, casting doubt on whether they can achieve true quantum utility. In contrast, generative learning frameworks are not constrained by this limitation, making them particularly promising candidates for demonstrating quantum computational advantage.

Early attempts at classically training quantum generative models relied on estimating global output probabilities [22], which limits scalability. Building on trainability results for generative models, the authors of Ref. [23] proposed an expectation-value-based formulation of the squared maximum mean discrepancy (MMD²) loss function that was later used to construct a scalable training framework for parametrized IQP circuits [24, 25]. Subsequent work established universality of such models under additional resources [26]. More recently, an alternative architecture, called Fermionic Born Machine [27], was introduced, providing a classically trainable generative model based on the Fermion Sampling quantum advantage scheme [28].

In this work, we take a step away from qubit-based QML models and introduce *Gaussian Bosonic Born Machines* (GBBMs), which form a class of classically trainable quantum generative models inspired by Gaussian Boson Sampling [29, 30]. Our approach primarily employs parity-operator strings as observables, which play a role analogous to Pauli- Z operators in qubit-based models and enable an expectation-value formulation of the MMD² loss in the bosonic setting. Crucially, this allows the loss to be evaluated efficiently using only the first and second moments of the Gaussian state, avoiding explicit sampling during training, while still retaining sampling hardness in the appropriate regimes [29, 31, 32]. The overall training and inference workflow of the GBBM is depicted in Fig. 1.

Beyond trainability, photonic architectures are also attractive from a hardware perspective. Photonic experiments can operate at repetition rates in the range 1-100 MHz, as set by optical

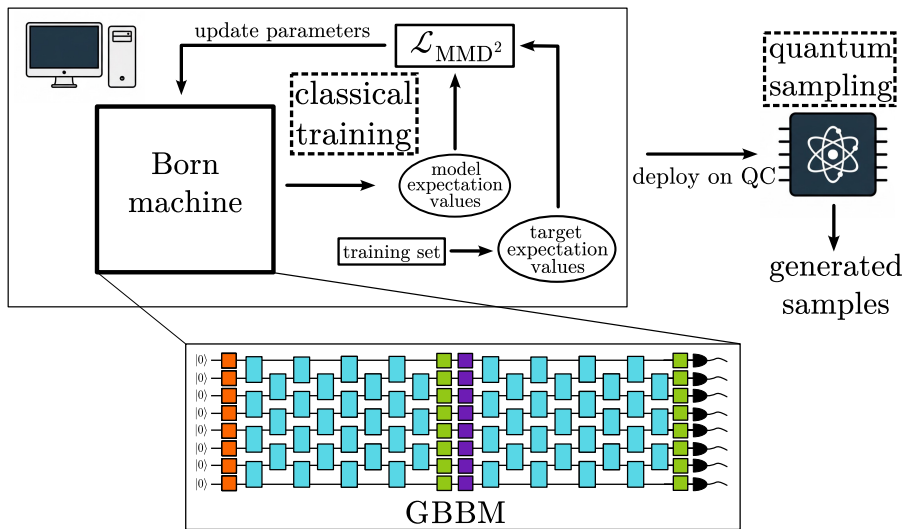


Figure 1: Schematic overview of the Gaussian Bosonic Born Machine (GBBM) framework. During *classical training*, the Born machine is optimized by minimizing an $\mathcal{L}_{\text{MMD}}^2$ loss between model and target expectation values computed from the training set. After classical training, the learned GBBM is deployed for *quantum sampling*, where measurements on the quantum device produce generated samples.

source and detector technologies [33, 34]. In contrast, while qubit-based platforms support gate operations on nanosecond timescales, the effective inference rate for complete circuit execution (including measurement and reset) is typically limited to the kilohertz regime on current devices [35–37]. This separation in achievable repetition rates suggests that photonic platforms may offer substantially higher inference throughput in near-term implementations. In addition, Gaussian Boson Sampling architectures appear particularly promising from a scalability perspective, as illustrated by recent large-scale demonstrations on the Jiuzhang 4.0 processor using 1024 input squeezed states and 8176 output modes [34].

The paper is organized as follows. In Section 2, we review the preliminaries, introduce the GBBM model and derive the parity operator and threshold operator formulation of the MMD^2 training objective. Subsequently, Section 3 details the classical training algorithm for the GBBM based on parity operators. In Section 4, we present a numerical benchmark demonstrating scalability and practical performance with up to 805 bosonic modes, and more than 10^6 trainable parameters. Finally, we conclude in Section 5 with a discussion of limitations, experimental considerations, and possible extensions beyond the Gaussian setting.

2 Framework of Gaussian Bosonic Born Machines

This section presents a framework for classically trainable Born machines in the bosonic setting by employing Gaussian states. First, we provide the necessary background on bosonic Gaussian states, Gaussian Boson Sampling and classical training strategies adapted to a photonic domain. We then present a reformulation of the MMD² loss function using operator expectation values relevant in bosonic systems. Finally we introduce our generative model construction, which is designed to be trained efficiently using classical computing resources and deployed on quantum hardware.

2.1 Gaussian states and Gaussian Boson Sampling

Here we give a basic introduction of relevant concepts needed for introducing our proposed quantum generative model. For a more detailed background on Gaussian states we refer to Refs. [38, 39] and Appendix A; concerning Gaussian Boson Sampling, we refer to Refs. [29, 30].

Gaussian states represent a fundamentally important and experimentally accessible class of continuous-variable quantum states. In particular, they can be fully characterized by their displacement vector $\boldsymbol{\mu}$ and covariance matrix Σ defined elementwise by

$$\begin{aligned}\mu_i &:= \text{Tr}[\rho \hat{\chi}_i], \\ \Sigma_{ij} &:= \text{Tr}[\rho \{\hat{\chi}_i - \mu_i \mathbb{1}, \hat{\chi}_j - \mu_j \mathbb{1}\}],\end{aligned}\tag{1}$$

where $\{A, B\} := AB + BA$ is the anticommutator and $\boldsymbol{\chi}$ is a vector of quadrature operators defined as $\boldsymbol{\chi} = [\hat{\chi}_1, \dots, \hat{\chi}_{2d}]^T = [\hat{x}_1, \dots, \hat{x}_d, \hat{p}_1, \dots, \hat{p}_d]^T$. We call Gaussian states with displacement vector $\boldsymbol{\mu} = \mathbf{0}$ *centralized* (or non-displaced) Gaussian states.

First introduced in Refs. [29, 30], the Gaussian Boson Sampling protocol demonstrates quantum advantage by sampling the photon-number distribution of a randomly generated Gaussian state. Similarly to standard Boson Sampling with Fock-state inputs [40], generating samples from these photonic output distributions is widely believed to be classically hard in the relevant parameter regimes. The complexity of taking a sample from a centralized Gaussian state is characterized by the evaluation of a matrix function called the hafnian [41], which, in general, is a difficult task using classical resources. Hence, it is widely believed that performing an ideal Gaussian Boson Sampling experiment is intractable on a classical computer [32, 42].

Traditionally, Gaussian Boson Sampling experiments use photonic circuits composed of squeezing gates and multimode interferometers [34, 43–45], resulting in pure centralized Gaussian states in ideal conditions. However, as we explain in the subsequent sections, our circuit ansatz also uses displacement gates, resulting in displaced Gaussian states. Consequently, the probability distribution corresponding to the particle-resolved particle number detection is characterized by the loop hafnian [46, 47]. This is a generalization of the conventional Gaussian Boson Sampling experiment, hence, it is also believed to be classically intractable to simulate in low-displacement regimes [32].

The current state-of-the-art classical simulation of an ideal Gaussian Boson Sampling experiment can be found in Ref. [48]. However, as realistic Gaussian Boson Sampling experiments are currently lossy, one can make the sampling algorithm more efficient by incorporating these losses into the classical sampling algorithm [31, 49]. It should be noted, that local noise in large quantum circuits may have the effect of strongly suppressing higher-order correlations, which also leads to an efficient algorithm for reproducing experimental Gaussian Boson Sampling data [50].

2.2 Training quantum generative models using MMD²

Generative modeling aims to learn a parameterized probability distribution $q_{\mathbf{w}}$ that approximates a target distribution p , so that samples drawn from $q_{\mathbf{w}}$ are statistically similar to those drawn from p . Accordingly, the representation should be paired with a protocol that enables efficient sampling from $q_{\mathbf{w}}$.

At the heart of our approach lies the concept of *Quantum Circuit Born Machines* (QCBMs), where the model distribution is implemented using a parametrized quantum circuit followed by a relevant measurement on all qubits [51–53], targeting generative problems over d binary random variables. In a typical qubit setting, a QCBM is characterized by a circuit ansatz $U(\mathbf{w})$ with trainable parameters \mathbf{w} . Measurement of all qubits in the computational basis defines the model distribution through the Born rule

$$q_{\mathbf{w}}(\mathbf{x}) = \text{Tr}[U(\mathbf{w}) |\mathbf{0}\rangle\langle\mathbf{0}| U^\dagger(\mathbf{w}) M_{\mathbf{x}}], \quad (2)$$

where \mathbf{x} is a bitstring with $x_i \in \{0, 1\}$ and $M_{\mathbf{x}} = |\mathbf{x}\rangle\langle\mathbf{x}| = \bigotimes_{i=1}^d |x_i\rangle\langle x_i|$. The parameters are optimized by minimizing a suitable loss so that the generated samples match the training data. Similarly, photonic QCBMs [54] are obtained by initializing the system in a d -mode vacuum state instead of $|\mathbf{0}\rangle$, implementing $U(\mathbf{w})$ as a photonic circuit ansatz, and defining $M_{\mathbf{x}}$ as the projector onto measurement outcome patterns labeled by \mathbf{x} . It is worth noting that continuous-variable Born machines can also be realized in photonic systems through homodyne measurements [55, 56], which provide a continuous-outcome alternative to our discrete measurement schemes.

Besides the choice of ansatz, another important building block in this framework is the loss function. Explicit loss functions, such as the total variation distance (TVD) or the Kullback–Leibler (KL) divergence, are generally hard to estimate accurately from samples, with sample requirements that often scale poorly with dimension. This can make training prohibitively costly and may further worsen trainability issues such as barren plateaus [23]. A convenient alternative is the *squared maximum mean discrepancy* (MMD²), which is defined below [57]. In this work, we consider binary-valued outcomes $\mathbf{x} \in \{0, 1\}^d$, where x_i denotes the binary outcome of mode i . Let p and $q_{\mathbf{w}}$ be two probability distributions over outcomes $\mathbf{x} \in \{0, 1\}^d$, representing the target and model distributions, respectively. Given a kernel

function $K(\mathbf{x}, \mathbf{y})$, the MMD² between these two probability distributions is defined as

$$\text{MMD}^2(p, q_w) := \mathbb{E}_{\mathbf{x}, \mathbf{x}' \sim p} [K(\mathbf{x}, \mathbf{x}')] + \mathbb{E}_{\mathbf{y}, \mathbf{y}' \sim q_w} [K(\mathbf{y}, \mathbf{y}')] - 2\mathbb{E}_{\mathbf{x} \sim p, \mathbf{y} \sim q_w} [K(\mathbf{x}, \mathbf{y})], \quad (3)$$

where $K : \{0, 1\}^d \times \{0, 1\}^d \rightarrow \mathbb{R}$ is a kernel function. The Gaussian kernel

$$K_\sigma(\mathbf{x}, \mathbf{y}) := \exp\left(-\frac{\|\mathbf{x} - \mathbf{y}\|_2^2}{2\sigma}\right) = \prod_{i=1}^d \exp\left(-\frac{(x_i - y_i)^2}{2\sigma}\right) \quad (4)$$

is a natural choice for the MMD²-based training, since it is characteristic and thus uniquely specifies the underlying probability distribution [57].

As shown in Ref. [23], the MMD² loss can also be expressed using expectation values of Pauli- Z strings, which is a key observation leading to classically trainable models. However, to date, such reformulations of the loss function $\mathcal{L}_{\text{MMD}^2}(p, q_w)$ have been established primarily for qubit-based quantum systems, with a straightforward extension to fermionic models [27]. For our purposes, we need to generalize this formulation to the bosonic setting. We can start by considering projective measurements with binary outcomes labeled by $\mathbf{x} \in \{0, 1\}^d$, where the j th element x_j corresponds to a binary outcome on mode j . From such projectors $M_{\mathbf{x}}$ we can define the observable O_A as

$$O_A := \sum_{\mathbf{x} \in \{0, 1\}^d} (-1)^{|\mathbf{x}_A|} M_{\mathbf{x}} = \bigotimes_{j \in A} (M_0^{(j)} - M_1^{(j)}) \otimes \mathbb{1}_{[d] \setminus A} \quad (5)$$

where $A \subseteq [d]$ is a subset of modes and \mathbf{x}_A denotes the vector formed from x according to the indices in A and $|\mathbf{x}_A|$ denotes the Hamming weight of \mathbf{x}_A . As detailed in Appendix B, using Equation (5), we can rewrite the MMD² expression as

$$\mathcal{L}_{\text{MMD}^2}(p, q_w) = \mathbb{E}_{A \sim p_K} \left[(\langle O_A \rangle_p - \langle O_A \rangle_{q_w})^2 \right], \quad (6)$$

where $\langle O_A \rangle_p$ and $\langle O_A \rangle_{q_w}$ denote expectation values of the operator string O_A under the target and model distributions, respectively. In this expression, K denotes the kernel and p_K the corresponding distribution induced over operator strings, given by

$$p_{K_\sigma}(A) = (1 - p_\sigma)^{d-|A|} p_\sigma^{|A|}, \quad (7)$$

where $p_\sigma := \frac{1}{2}(1 - e^{-1/2\sigma})$.

To generalize this procedure for bosonic systems, we define two natural projective measurements that provide binary outcomes suitable for the MMD² reformulation. These analogs to the qubit Z -measurement represent common detection schemes in quantum optics:

1. **Parity detection** [58]: distinguishes between even and odd particle numbers, defined by the single-mode measurement projectors

$$M_0 = \sum_{k=0}^{\infty} |2k\rangle\langle 2k|, \quad M_1 = \mathbb{1} - M_0. \quad (8)$$

2. **Threshold detection** [59]: differentiates between the vacuum state (“no-click”) and all excited states (“click”), defined by the single-mode measurement projectors

$$M_0 = |0\rangle\langle 0|, \quad M_1 = \mathbb{1} - M_0. \quad (9)$$

Both of these measurement schemes effectively “discretize” the infinite-dimensional bosonic Hilbert space into a format compatible with the MMD²-based training of QCBMs. Moreover, both of these measurements are feasible to perform in a physical experiment; parity detection is extensively used in the Wigner tomography of quantum states [60, 61], while threshold detection can be performed with single-photon detectors that are inexpensive and can be operated at room temperature [62].

2.3 Gaussian Bosonic Born Machines

Inspired by the Gaussian Boson Sampling quantum advantage proposal and recent progress in classically trainable quantum generative models, we propose *Gaussian bosonic Born machines* (GBBMs), a class of photonic QCBMs formally defined as follows:

Definition 1 (Gaussian Bosonic Born Machine). A GBBM on d bosonic modes is a quantum generative model with the following components:

1. **Initial state:** an arbitrary Gaussian state, conveniently the vacuum state $|0\rangle$;
2. **Variational circuit:** a parameterized photonic quantum circuit composed of Gaussian operations, including multiport interferometers, squeezing and displacement gates;
3. **Measurement:** terminal particle number measurements performed on each mode, which is coarse-grained to yield a discrete bitstring-valued probability distribution.

Our construction of the variational circuit ansatz follows the continuous-variable quantum neural network architecture proposed in Ref. [63], but restricts the model to linear transformations by omitting the Kerr nonlinearity. Note that, although multiple layers are formally redundant when only linear transformations are used, their inclusion can still improve the optimization behavior of the model; see the discussion below. We write the parameter vector as $\mathbf{w} := (\mathbf{w}^{(1)}, \dots, \mathbf{w}^{(L)})$ with L being the number of layers in the ansatz and each layer indexed by k is described by

$$\mathbf{w}^{(k)} := (\boldsymbol{\alpha}^{(k)}, \boldsymbol{\theta}_1^{(k)}, \mathbf{r}^{(k)}, \boldsymbol{\theta}_2^{(k)}), \quad (10)$$

where

1. $\boldsymbol{\alpha}^{(k)} \in \mathbb{R}^d$ is a displacement in the position direction,
2. $\boldsymbol{\theta}_1^{(k)} \in [0, 2\pi)^{d^2}$ defines the first interferometer by $U_1^{(k)} := U(\boldsymbol{\theta}_1^{(k)}) \in U(d)$,

3. $\mathbf{r}^{(k)} \in \mathbb{R}^d$ are squeezing parameters of the squeezing gates,
4. $\boldsymbol{\theta}_2^{(k)} \in [0, 2\pi)^{d^2}$ defines the second interferometer by $U_2^{(k)} := U(\boldsymbol{\theta}_2^{(k)}) \in U(d)$.

The interferometers are parameterized using standard linear-optical decompositions. In this work, we employ the Clements decomposition [64], although the Reck decomposition [65] could be used equivalently. Although most Gaussian Boson Sampling experiments focus on centered Gaussian states, incorporating displacement gates into the circuit ansatz removes this restriction and substantially enhances the expressivity of the model. Hence, in total, a single layer of the resulting ansatz containing the Clements interferometer layout has $2d^2 + 2d$ trainable parameters.

We further note that this variational circuit implements a Bloch-Messiah decomposition [66] and is therefore universal for preparing arbitrary pure Gaussian states with a single layer from the vacuum state. However, the brickwork structure of this ansatz limits information spreading during training. To overcome this obstacle, we first adapt the method discussed in Ref. [27] for a fermionic case and implement multiple layers with independent trainable parameters. This technique was found to enhance the optimization properties of the model associated with overparameterization, while still retaining an efficient classical description of the Gaussian state via its mean vector and covariance matrix. To extend these results, we also introduce an alternative ansatz construction that, instead of a brickwork architecture, implements two-mode gates via beamsplitters along a pre-defined arbitrary graph (with edge ordering specified due to the non-commuting nature of the beamsplitters). As we show in our numerical demonstrations, this can be used to improve information spreading while providing additional flexibility in choosing the number of trainable parameters.

The expectation values of the required operator strings can be computed efficiently on a classical computer; the specific details of this procedure are presented in the next section. Once classical training is complete, the resulting circuit ansatz provides a full description of a pure Gaussian state. In particular, this state can be compiled on a photonic processor using only $\mathcal{O}(d^2)$ linear optical gates in the worst case, a complexity that remains independent of the number of layers used during the classical optimization phase. For inference, the optimized parameters are deployed onto a photonic quantum device equipped with photon number detectors. To generate the discrete data, we only use a coarse-graining of the raw photon counts, possibly circumventing the experimental requirement for photon-number-resolving detectors. Specifically, we consider two types of detectors: parity detectors, governed by the transformation $n \mapsto \frac{1}{2}(1 - (-1)^n)$ where n is the raw photon count; and threshold detectors, defined by the mapping

$$n \mapsto \begin{cases} 0 & n = 0, \\ 1 & n \geq 1. \end{cases}$$

Either choice of detector effectively transforms the underlying Gaussian state into a discrete bitstring distribution suitable for generative modeling tasks.

The threshold variant of Gaussian Boson Sampling is widely believed to be computationally intractable to simulate classically [59]. Because parity and threshold measurements are equivalent in the dilute regime—where the number of modes scales at least quadratically with the total number of photons—this computational hardness naturally extends to the parity-based variant. Note, however, is that sufficiently large displacements can induce a complexity transition, rendering the sampling task classically efficient [32]. Moreover, the initial training parameters are typically chosen so that the average photon number of the resulting state scales linearly with the number of modes. Assuming, in addition, that the training data are such that the average Hamming weight scales linearly with the bitstring length, we expect quantum inference to typically operate in the linear regime (See Ref. [67] for proofs of hardness of Boson Sampling and Bipartite Gaussian Boson Sampling with particle number detectors).

3 Efficient classical training of parity GBBMs

We continue by presenting an efficient classical training algorithm for GBBMs based on parity operator strings. The key observation is that expectation values of parity strings on Gaussian states can be computed efficiently on a classical computer, independent of string length. Consequently, GBBMs admit an efficient classical training method.

Our approach starts by tracking the evolution of the mean vector $\boldsymbol{\mu}$ and the covariance matrix Σ of the underlying Gaussian quantum state. The input state is the vacuum state, characterized by

$$\boldsymbol{\mu} = \mathbf{0}, \quad \Sigma = \mathbb{1}_{2d}, \quad (11)$$

and we apply a sequence of L parameterized Gaussian transformations corresponding to the layers of the photonic circuit. The Gaussian state parameters transform under each layer as

$$\boldsymbol{\mu} \mapsto S\boldsymbol{\mu} + \boldsymbol{r}, \quad \Sigma \mapsto S\Sigma S^T, \quad (12)$$

where \boldsymbol{r} is the displacement vector and S is the real symplectic matrix associated with the corresponding Gaussian operation (composed of interferometers and squeezing). Since each update in Equation (12) involves matrix multiplications of size $2d \times 2d$, the full evolution of the state can be simulated classically in $\mathcal{O}(Ld^3)$ time, where L is the number of layers.

After computing the final Gaussian state, we evaluate the parity-operator expectation values required for the loss function defined in Eq. (6). During training, a fixed number of parity-operator strings are sampled from the distribution specified by the Gaussian kernel from Eq. (7). As discussed in Appendix C, the expectation value of a parity-string operator Π_A , acting on a subset of modes $A \subseteq [d]$, admits a closed-form expression:

$$\text{Tr}[\Pi_A \rho] = \frac{\exp(-\boldsymbol{\mu}_A^T \Sigma_A^{-1} \boldsymbol{\mu}_A)}{\sqrt{\det \Sigma_A}}, \quad (13)$$

where $\boldsymbol{\mu}_A$ and Σ_A denote the mean vector and covariance matrix of the reduced Gaussian state $\text{Tr}_{[d] \setminus A}[\rho]$, obtained by restricting $\boldsymbol{\mu}$ and Σ to the modes indexed by A . Crucially, this

formula allows parity-string expectation values to be computed efficiently using only elementary numerical methods. For a parity string of length $\ell = |A|$, the computational cost of evaluating the corresponding expectation value scales as $\mathcal{O}(\ell^3)$, dominated by the inversion (or Cholesky factorization) of the reduced covariance matrix Σ_A . In practice, however, $\ell \ll d$ for the parity strings of interest, so this step is typically inexpensive. Instead, the overall computational cost might often be dominated by the construction of the full covariance matrix of the d -mode Gaussian state. As a result, expectation value estimation remains scalable even for photonic systems with a large number of modes, with the bottleneck shifting from the parity string expectation value evaluation to the covariance matrix construction. Using the backpropagation algorithm, these observations allow for efficient gradient computation. This is summarized in the following theorem.

Theorem 1 (Classical trainability of parity GBBMs). For a GBBM over d bosonic modes, as defined in Definition 1, the expectation value of any length- ℓ parity string $\text{Tr}[\Pi_A \rho]$ can be evaluated classically in $\mathcal{O}(\ell^3)$ time, given the corresponding mean vector and covariance matrix characterizing the final Gaussian state. Moreover, these objects can be obtained in $\mathcal{O}(Ld^3)$ time using $\mathcal{O}(d^2)$ memory, where L is the number of layers. Consequently, the model admits efficient classical training via automatic differentiation and backpropagation using an approximation of the MMD^2 loss function.

Proof. Evaluating Equation (13) takes $\mathcal{O}(\ell^3)$ time, as the computation time is dominated by the determinant in the denominator. Storing all the data characterizing a Gaussian state requires $\mathcal{O}(d^2)$ memory, which is also sufficient for computing the final covariance matrix from the initial covariance matrix using in-place updates. Updating the covariance matrix requires $\mathcal{O}(Ld^3)$ steps, because applying an interferometer to a Gaussian state amounts to an update of the covariance matrix requiring $\mathcal{O}(d^3)$ time. \square

For completeness, we also provide a rough sketch of the proposed algorithm for estimating MMD^2 in Algorithm 1. The algorithm works by computing the mean vector $\boldsymbol{\mu}$ and the covariance matrix Σ of the Gaussian state from the ansatz parameters \boldsymbol{w} . From the Gaussian state representation we can compute the expectation value of each parity string, while the target expectation values are obtained from the bitstrings sampled from the target distribution p . The average squared difference between the model and target expectation values yields the final MMD^2 estimate.

Algorithm 1 Classical evaluation of the MMD² for a parity GBBM

Require: Parameters $\mathbf{w} = (\mathbf{w}^{(1)}, \dots, \mathbf{w}^{(L)})$, with $\mathbf{w}^{(k)} = (\boldsymbol{\alpha}^{(k)}, \boldsymbol{\theta}_1^{(k)}, \mathbf{r}^{(k)}, \boldsymbol{\theta}_2^{(k)})$; bitstrings $\{\mathbf{x}^{(n)}\}_{n=1}^N$ sampled from the target distribution p ; Gaussian kernel bandwidth σ ; number of parity strings M .

Ensure: Estimate of $\mathcal{L}_{\text{MMD}}(p, q_w)$.

```
1:  $\boldsymbol{\mu} \leftarrow \mathbf{0}, \quad \Sigma \leftarrow \mathbb{1}_{2d}$  ▷ Vacuum state initialization
2: for  $k = 1, \dots, L$  do ▷ Compute Gaussian state using Equation (12)
3:    $U_1^{(k)} \leftarrow U(\boldsymbol{\theta}_1^{(k)}), \quad U_2^{(k)} \leftarrow U(\boldsymbol{\theta}_2^{(k)})$ 
4:   Construct the symplectic matrix  $S^{(k)}$  from  $(U_1^{(k)}, \mathbf{r}^{(k)}, U_2^{(k)})$ 
5:   Construct the displacement vector  $\mathbf{t}^{(k)}$  from  $\boldsymbol{\alpha}^{(k)}$ 
6:    $\boldsymbol{\mu} \leftarrow S^{(k)} \boldsymbol{\mu} + \mathbf{t}^{(k)}$  ▷ Evolve displacement vector
7:    $\Sigma \leftarrow S^{(k)} \Sigma (S^{(k)})^T$  ▷ Evolve covariance matrix
8: end for
9:  $S \leftarrow 0$ 
10: for  $m = 1, \dots, M$  do ▷ Compute parity string expectation values
11:   Sample  $A$  from  $p_{K_\sigma}$  corresponding to a parity string
12:    $\langle \Pi_A \rangle_p \leftarrow \frac{1}{N} \sum_{n=1}^N (-1)^{|\mathbf{x}_A^{(n)}|}$  ▷ Compute target parity
13:   Obtain  $(\boldsymbol{\mu}_A, \Sigma_A)$  by restricting  $(\boldsymbol{\mu}, \Sigma)$  to modes in  $A$ 
14:    $\langle \Pi_A \rangle_{q_w} \leftarrow \exp(-\boldsymbol{\mu}_A^T \Sigma_A^{-1} \boldsymbol{\mu}_A) / \sqrt{\det(\Sigma_A)}$  ▷ Compute model parity using Equation (13)
15:    $S \leftarrow S + \left[ \langle \Pi_A \rangle_p - \langle \Pi_A \rangle_{q_w} \right]^2$ 
16: end for
17: return  $S/M$  ▷ Return the MMD2 estimate
```

4 Numerical experiments

In this section, we demonstrate the scalability of our generative model and training framework, benchmarking it against well-established classical methods. We first introduce all models and their tunable hyperparameters, followed by describing the benchmark datasets together with the corresponding training and test results. All GBBM trainings rely on our Python implementation [68] written using JAX [69] for automatic differentiation. These demonstrations aim to study certain important aspects of our framework as well as to compare the performance to classical models. In our assessment of a trained models performance, we rely on two metrics: the covariance matrix of the corresponding probability distributions for visual investigations, and the MMD² evaluated with respect to a test set using different σ bandwidths. The covariance matrix of a probability distribution p (not to be confused with the covariance matrix of a Gaussian state) is defined elementwise as

$$[\text{cov}_p]_{ij} := \mathbb{E}_{\mathbf{x} \sim p}[x_i x_j] - \mathbb{E}_{\mathbf{x} \sim p}[x_i] \mathbb{E}_{\mathbf{x} \sim p}[x_j]. \quad (14)$$

Since we do not have access to the true underlying probability distribution of the target datasets, but only to finite set of training and test samples, the visualized covariance matrices for the data are necessarily empirical estimates. In contrast, for a trained GBBM parameterized by a Gaussian state ρ , the exact analytical covariance matrix of the generated distribution can be computed directly from the expectation values of local operators.

4.1 Benchmark models

4.1.1 GBBM models

We use a varying number of layers and interferometer layouts for the GBBM model as in Definition 1, where the beamsplitter and phaseshifter angle parameters are initialized uniformly at random from $[0, 2\pi)$, and the displacement and squeezing amplitudes are drawn from a normal distribution $\mathcal{N}(0, 0.1)$. Besides choosing the right σ bandwidths for the Gaussian kernel function from Equation (4) (using the median heuristic from Ref. [70]), here we also tune the learning rate and the number of training iterations. While compatible with both gradient-based and gradient-free optimizers, in our implementation, we tune the parameters using the Adam optimizer [71]. Our model relies primarily on terminal parity measurements, but we also showcase an alternative strategy in Section 4.5 based on threshold detection.

4.1.2 Restricted Boltzmann machine

As a classical baseline learning model, we consider the *Restricted Boltzmann Machine* (RBM) architecture [72, 73]. RBMs form a class of energy-based models defined on a bipartite graph comprising n visible and m latent binary variables. Given a weight matrix W and bias vectors \mathbf{a}, \mathbf{b} , the energy of the system is given by

$$E(\mathbf{v}, \mathbf{h}) = -\mathbf{a}^T \mathbf{v} - \mathbf{b}^T \mathbf{h} - \mathbf{v}W\mathbf{h}, \quad (15)$$

where \mathbf{v} and \mathbf{h} denote the state of the visible and hidden units. This energy function determines the joint probability distribution according to the Boltzmann distribution

$$q(\mathbf{v}, \mathbf{h}) = \frac{1}{Z} e^{-E(\mathbf{v}, \mathbf{h})}, \quad (16)$$

where Z is the normalization constant. The probability of observing a specific visible state \mathbf{v} is obtained by marginalizing over the latent space:

$$q(\mathbf{v}) = \sum_{\mathbf{h}} q(\mathbf{v}, \mathbf{h}). \quad (17)$$

Our training procedure adopts the strategy from Ref. [25], using persistent contrastive divergence via scikit-learn’s `BernoulliRBM` class [74, 75]. As a key hyperparameter, we scan the number of hidden units $m \in [\lfloor n/2 \rfloor, n]$ and choose the architecture that minimizes the MMD² metric across various bandwidths σ .

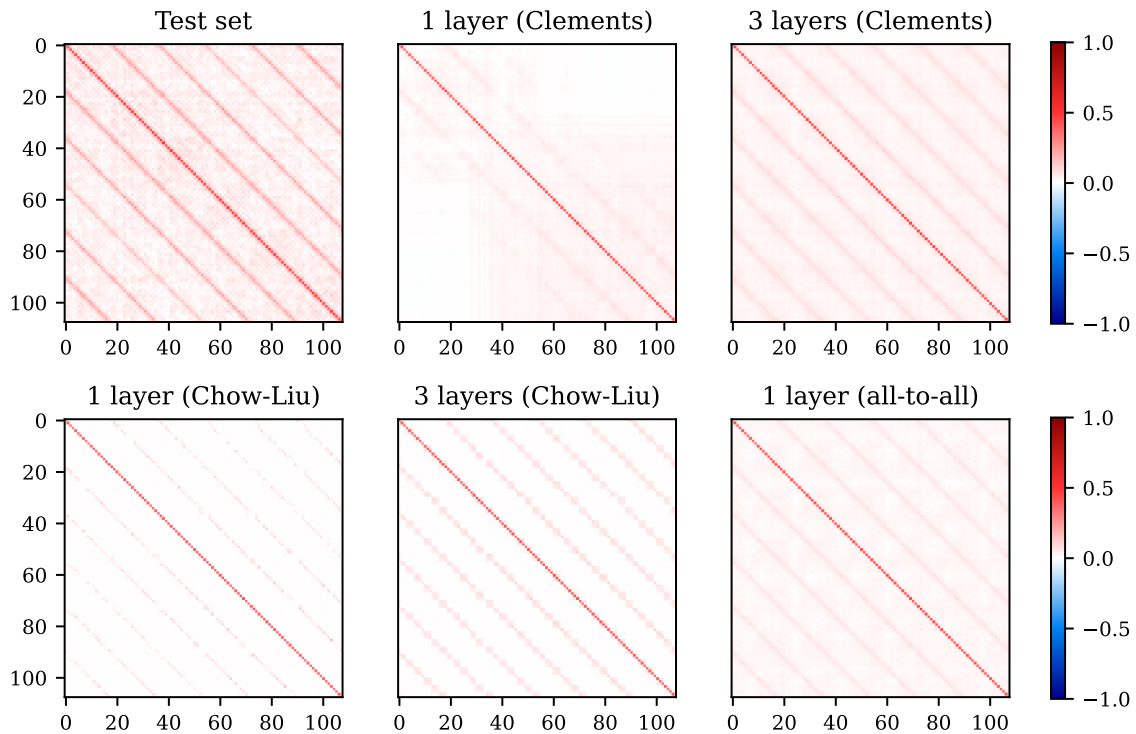


Figure 2: **The effect of ansatz choice on the performance GGBMs.** The models were trained on the equilibrium states of a cellular automaton over a 6×12 grid. GGBMs were constructed with an increasing number of layers and different interferometer layouts (Clements, Chow-Liu and all-to-all layouts).

4.1.3 Empirical Chow-Liu tree approximation

To capture the basic statistics of the dataset, we construct a tree-structured Bayesian network using the Chow-Liu algorithm [76] via the `pgmpy` library [77]. This method approximates the joint distribution by maximizing mutual information to form a maximum weight spanning tree, rooting it at the first variable, and fitting parameters through maximum likelihood estimation. The resulting tree topology allows for efficient and exact sampling because each node has a single parent. We evaluate the performance of the model by measuring the MMD^2 distance between a large, fixed-size set of samples and the original test set. Although this provides a computationally efficient baseline, its accuracy is limited to smaller problems or datasets that align with a tree-like correlation structure.

4.2 Exploring overparametrization and alternative ansätze

Similarly to the method described in Ref. [27], we start by investigating the effect of including multiple layers in the GBBM model, but also extend it to alternative interferometer layouts. For this, we consider a dataset constructed from the equilibrium states of a *cellular automaton* (CA) on a 6×18 grid. The samples were obtained by starting the CA in different uniformly random states and evolving them for 1000 steps under Conway’s Game of Life rules [78], then storing the final state. This process was repeated several times to collect a training and test set of 1000 samples each, after disregarding the all-0 states. We present a few examples from the training dataset in Appendix F.

The GBBMs were trained for 5000 episodes with an initial learning rate of 0.001, using two kernel bandwidths $\sigma \in \{8.72, 17.44\}$. We start by studying the information spreading in the GBBM ansatz and analyze the covariance matrix of the trained models. We consider 3 distinct interferometer layouts in our experiments. The first is based on the Clements decomposition described in Section 2.3; a single layer having 23544 trainable parameters in this case (108 modes). The other two layouts are constructed from a pre-specified graph by applying beamsplitters between mode pairs corresponding to the ordered set of edges, inspired by the probabilistic graphical model approach of [79]. We consider two extreme cases: a tree graph obtained using the Chow-Liu approximation of the dataset and a complete graph, where the edge-ordering corresponds to a uniformly random permutation. A single layer in the ansatz constructed using these graphs admits 860 and 11664 parameters, respectively.

The covariance matrices of the trained models are shown in Fig. 2, where Chow-Liu and all-to-all refer to the tree and complete graph interferometer layouts. These results signify the importance of the choice of parametrization of Gaussian states in the context of generative learning. The observation that a single layer obtained using the Clements layout is close to diagonal and that this can be improved by including multiple layers is consistent with the fermionic case, noted by the authors in Ref. [27]. In the current work, however, we extend these results by showing that alternative parametrizations (with significantly less parameters) can be used to circumvent this unwanted concentration and improve information spreading during training. Even a single layer with the Chow-Liu interferometer layout lacks the covariance concentration behaviour exhibited by the Clements layout (while potentially introducing other biases), despite a 27-fold reduction of the number of trainable parameters.

4.3 USPS handwritten digit experiment

For our second experiment, we consider 16×16 grayscale images from the USPS dataset of handwritten digits [80]. The images are flattened and binarized to obtain bitstrings of length 256 and divided into a training set of size 19999 and a test set of 1500 samples. A few examples of the binarized training set are shown in Appendix. F.

The fine-tuned GBBM has 3 layers of the all-to-all interferometer layout as in the previous section, having 394752 trainable parameters in total. The model was trained with a learning

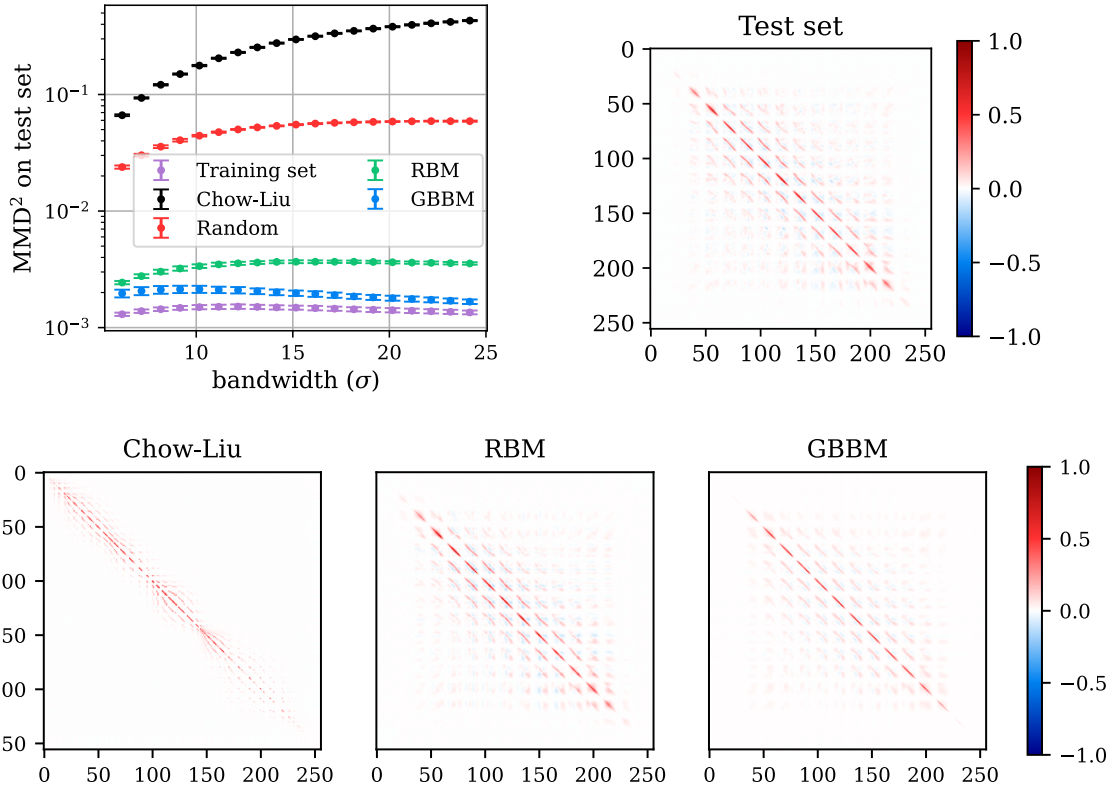


Figure 3: **Test results on the USPS dataset.** The dataset containing 16×16 grayscale images was converted into 256-long bitstrings. A GBBM was trained with 3 layers of the all-to-all interferometer layout and the fine-tuned RBM was trained with 188 hidden units for comparison. Markers denote mean values from 5 independent estimates and errorbars denote the corresponding standard deviations.

rate of 0.001 for 5000 episodes. The MMD^2 loss was estimated for three bandwidths $\sigma \in \{6.16, 12.33, 24.66\}$ using 10^4 parity strings each. For comparison, we trained an RBM with 188 hidden units, where this number was chosen as the best performing in the tuning range. The test results, obtained using 5 independent estimates for each σ bandwidths, are shown in Fig. 3. Our GBBM model achieves good results, outperforming the fine-tuned RBM model. The Chow-Liu approximation completely fails, showing worse MMD^2 values than the uniformly random samples, as the dataset does not exhibit a strong tree correlation structure.

4.4 Genomic experiment

For a large scale benchmark, we consider a genomic dataset containing bitstrings of length 805, where each bit in the sample indicates the presence or absence of the variant allele in the given

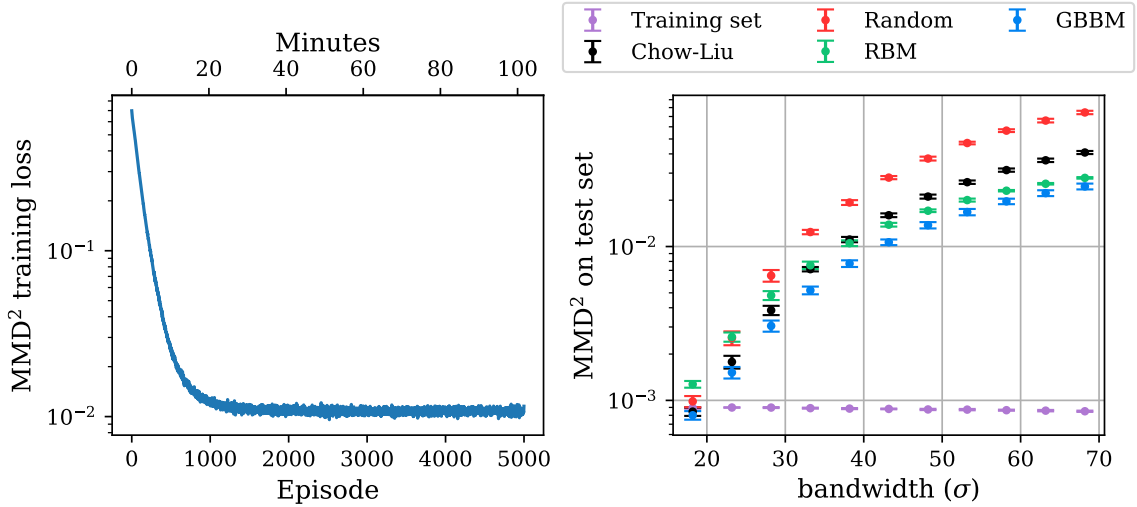


Figure 4: **Test results on the genomic dataset.** The models were trained on 805-bit long bitstrings. GBBMs have a single layer with 1297660 trainable parameters, and we trained an RBM with 492 hidden units for comparison. Markers denote mean values from 5 independent estimates and errorbars denote the corresponding standard deviations.

individual [25, 81, 82]. This dataset contains 5008 samples collected from 2004 individuals from the Human Genome Project and is divided into training and test datasets with a ratio of 1:3.

We first train a GBBM with 805 photonic modes using a single layer with the Clements interferometer layout, having 1,297,660 trainable parameters. The learning rate is set to 10^{-3} , and the model is trained for 5000 episodes, although convergence is reached in less than 2000 steps. In each training step, we sample 3×10^4 parity strings from Equation (7) employing 3 different kernel bandwidths $\sigma \in \{18.11, 36.22, 72.44\}$ obtained using the median heuristic [70] and use the corresponding expectation values to compute the MMD² estimate. Notably, the entire training process completed in approximately 100 minutes using a single NVIDIA A100 GPU. The training curve in both the training episodes and time is shown in Fig. 4 (left).

For comparison, we also train a RBM with 492 hidden units selected via hyperparameter tuning. The RBM is trained for 1000 episodes with a learning rate of 10^{-2} . In addition, we also consider the Chow-Liu approximation of the dataset and uniformly random samples as comparisons, computing MMD² to the test set based on 10^5 samples. Finally, we also compute the MMD² between the training set and the test set, serving as the ground truth reference.

After training, we evaluate the MMD² of each model with respect to the test set for a range of σ kernel bandwidths and display the results in Fig. 4 (right). We emphasize that all these discrepancies were evaluated using the MMD² formulated as expectation values from Equation (6). Notably, our GBBM outperforms statistical approximations (Chow-Liu tree and uniformly random samples) and the RBM in the relevant bandwidth regime using a comparable hyperparameter tuning.

4.5 Threshold GBBMs can learn near-balanced datasets

There is a notable limitation of parity GBBMs arising from the nature of the parity operator. Since expectation values of parity-operator strings correspond to the central values of reduced Wigner functions, they can only take positive values. Negative values can be obtained by flipping the dataset; therefore, when the dataset is dominated by low or high Hamming weight samples, the model is expected to perform well, as demonstrated previously. However, for balanced datasets containing comparable numbers of 0s and 1s, the parity-based model is not sufficient on its own, as the expectation values cannot attain zero, and approximating zero requires higher energy. Although this limitation can be partially mitigated by classical post-processing, we instead consider an alternative coarse-graining of particle-number measurement outcomes based on threshold detection [47]. This threshold detection-based variant is expected to provide significantly improved performance on near-balanced datasets. The classical algorithm for estimating threshold-string expectation values is detailed in Appendix E, where we demonstrate that the enhanced expressivity of the model involves a trade-off regarding the scalability of the classical training process.

To demonstrate a generative learning problem, where the parity GBBM fails, we construct a balanced dataset using the Metropolis algorithm on a classical 2D Ising model with periodic boundary conditions. The coupling strength is set to $J = 1$ and we used an alternating local field with magnitude $h = 0.08$ on a 14×14 grid with periodic boundary condition. First, the model was initialised in a random state and evolved using the Metropolis algorithm for 10^6 steps. After this warmup, a sample was collected by taking a snapshot of the spin configuration after every 2000 steps until a dataset of $15 \cdot 10^3$ samples were collected which we divided into a training and test set with a 2 : 1 split. Crucially, the algorithm requires a temperature which we set to $T = 2.4$, close to the critical temperature of the 2D Ising model. As shown in Fig. 5 (top, left), the resulting dataset is not concentrated only on the low Hamming weight subspace.

We train the GBBMs and the RBM for 5000 episodes with a learning rate of 0.001 using 3 bandwidths $\sigma \in \{10.58, 21.16, 42.33\}$ derived from the median heuristic. However, since the runtime of the classical simulation algorithm depends exponentially on the locality of the threshold operator strings, we impose a cutoff at $\ell = 7$. We use this limit for training both types of GBBMs, and testing all models. Both GBBMs were constructed with 5 layers of the Clements ansatz. The MMD² scores and the final covariance matrices of the trained models are shown in Fig. 5. The parity GBBM fails to learn this dataset and produces similar results as uniformly random sampling. The tuned RBM performs even worse, but this can be associated with the limitations of contrastive divergence. Notably, this generative problem—close to the critical temperature—is notoriously hard for Boltzmann machines trained with contrastive divergence [83]. On the other hand the threshold GBBM shows good results and successfully learns to capture patterns in the dataset.

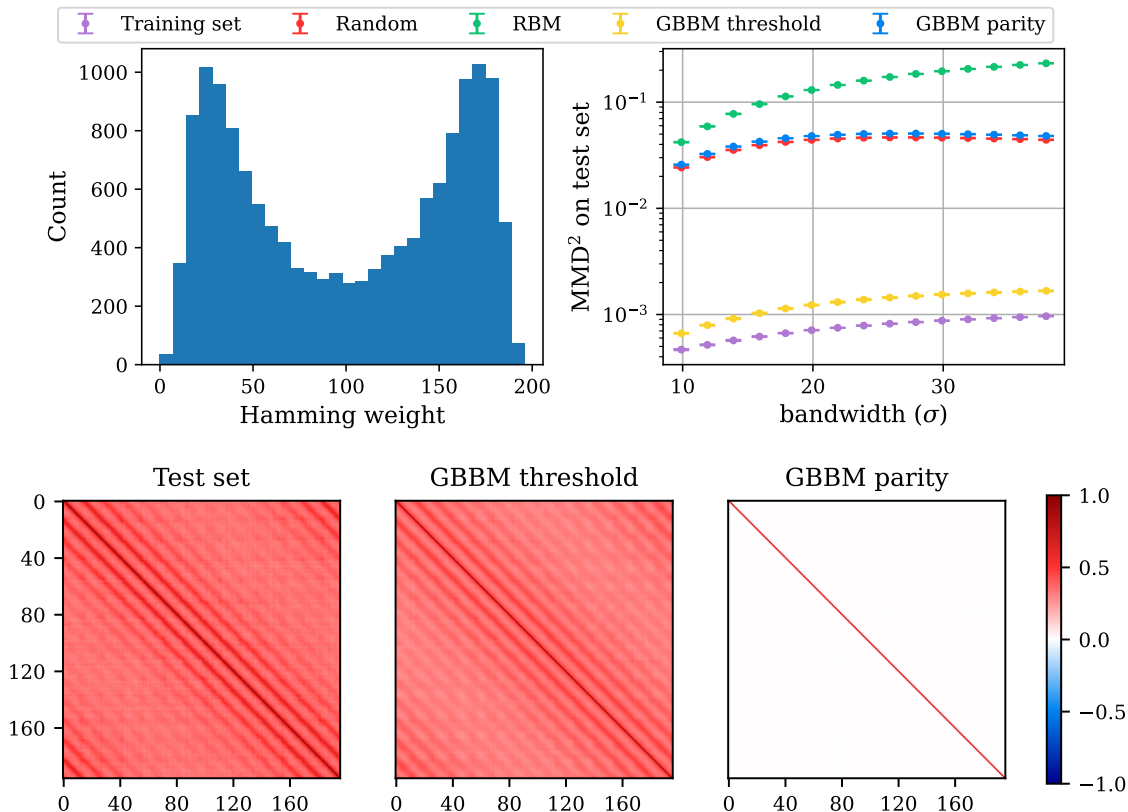


Figure 5: **Training parity and threshold GGBMs on the Ising dataset.** The models were trained with at most 7-long operator-string expectation values. (top, left) Distribution of the Hamming weight of training and test samples. (top, right) Truncated MMD² scores of the trained models evaluated up to locality 7. (bottom) Covariance matrices of the test set and the trained GGBMs.

5 Conclusion and outlook

In this work, we introduced a parity operator-based training framework for bosonic Gaussian quantum models that enables efficient classical evaluation of the MMD² loss while retaining a direct connection to experimentally realizable photonic platforms. Our parity-based approach imposes no intrinsic upper bound on the length of parity strings, with the computational cost governed instead by the number of modes and circuit layers. In particular, we demonstrated the practical scalability of the method by successfully training a model on a classical computer with up to 805 bosonic modes and 1,297,660 trainable parameters, using a single GPU in less than 2 hours. As Gaussian Boson Sampling experiments with thousands of modes are already available on current photonic hardware, our proposed framework is directly relevant to near-term implementations. Moreover, in such generative tasks, a key practical advantage of

photonic platforms over qubit-based architectures could be their inference throughput: while current qubit-based systems typically operate in the kilohertz regime, photonic implementations are expected to support substantially higher sampling rates [33, 34].

At the same time, realistic experimental conditions impose important constraints. In present-day photonic platforms, optical losses and other noise sources reduce the strength of observable correlations [50], which can limit the effective expressivity of the model. Nevertheless, training can still be performed in the presence of losses and learning can remain meaningful even when experimental imperfections are taken into account. Moreover, Gaussian Boson Sampling is believed to remain classically hard even in the presence of moderate loss [31], suggesting that useful generative models may be achievable without fully ideal hardware. Further reductions in experimental loss would make richer correlations accessible and could therefore improve the practical performance of the model.

Looking ahead, several directions merit further investigation. While parity and threshold operators constitute a robust and experimentally natural choice of observables, they capture only the coarsest nontrivial features of the resulting photon-number distribution. A natural generalization is to replace the operator strings in our framework with number-resolving observables, leading to a framework based on n -ary digits instead of bits. Understanding which classes of such observables admit efficient classical evaluation is an important open question. More broadly, it remains to be explored whether restricted forms of non-Gaussianity can be incorporated into the model, while preserving classical trainability. Additionally, one could shift the underlying quantum advantage scheme entirely; for instance, recent work has explored analogous generative frameworks based on standard Boson Sampling rather than Gaussian Boson Sampling [84, 85]. In general, identifying the boundary between enhanced expressivity and classical intractability will be crucial for the development of scalable and practically relevant photonic generative models.

6 Acknowledgement

ZK, BB and ZZ would like to thank the support of the Hungarian National Research, Development and Innovation Office (NKFIH) through the KDP-2023 funding scheme, the Quantum Information National Laboratory of Hungary and the grants TKP-2021-NVA-04, TKP2021-NVA-29 and FK 135220. MO acknowledges the support from the European Union’s Horizon Europe research and innovation program under EPIQUE Project GA No. 101135288. CO was supported by Global Partnership Program of Leading Universities in Quantum Science and Technology (RS-2025-08542968) through the National Research Foundation of Korea (NRF) funded by the Korean government (Ministry of Science and ICT(MSIT)). CO was also supported by the National Research Foundation of Korea Grants (No. RS-2024-00431768 and No. RS-2025-00515456) funded by the Korean government (Ministry of Science and ICT (MSIT)) and the Institute of Information & Communications Technology Planning & Evaluation (IITP) Grants funded by the Korea government (MSIT) (No. IITP-2025-RS-2025-02283189 and IITP-2025-

RS-2025-02263264). ZZ was partially supported by the Horizon Europe programme HORIZON-CL4-2022-QUANTUM-01-SGA via the project 101113946 OpenSuperQPlus100 and the QuantERA II project HQCC-101017733. ZZ also acknowledges funding from the Research Council of Finland through the Finnish Quantum Flagship project 358878. The C4QEC project is carried out within the IRAP of the Foundation for Polish Science co-financed by the European Union. The authors also acknowledge the computational resources provided by the Wigner Scientific Computational Laboratory (WSCLAB).

A Recap: Gaussian states

The current Appendix provides a brief overview of linear optics with an emphasis on Gaussian states and transformations; for comprehensive introductions, see Refs. [38, 39].

A Gaussian state ρ is a photonic quantum state fully characterized by the first and second moments of the quadrature operators $\hat{x}_1, \dots, \hat{x}_d, \hat{p}_1, \dots, \hat{p}_d$. These moments are collected into the mean vector $\boldsymbol{\mu} \in \mathbb{R}^{2d}$ and the covariance matrix $\Sigma \in \mathbb{R}^{2d \times 2d}$, defined elementwise as

$$\mu_i := \text{Tr}[\rho \hat{\chi}_i], \quad (18a)$$

$$\Sigma_{ij} := \text{Tr}[\rho \{\hat{\chi}_i - \mu_i \mathbb{1}, \hat{\chi}_j - \mu_j \mathbb{1}\}], \quad (18b)$$

where $\boldsymbol{\chi} = [\hat{\chi}_1, \dots, \hat{\chi}_{2d}]^T$ is the formal vector of quadrature operators defined as

$$\boldsymbol{\chi} := [\hat{x}_1, \dots, \hat{x}_d, \hat{p}_1, \dots, \hat{p}_d]^T, \quad (19)$$

and d is the number of bosonic modes. The quadrature operators satisfy the canonical commutation relations

$$[\hat{\chi}_i, \hat{\chi}_j] = i\Omega_{ij}, \quad (20)$$

where Ω is the canonical symplectic form

$$\Omega := \begin{bmatrix} 0 & \mathbb{1}_{d \times d} \\ -\mathbb{1}_{d \times d} & 0 \end{bmatrix}. \quad (21)$$

For Σ to describe a physical quantum state, it must be symmetric and satisfy the Robertson-Schrödinger uncertainty relation [38]

$$\Sigma + i\Omega \geq 0. \quad (22)$$

The bridge between the operator formalism and the phase-space representation of quantum optics is provided by the Weyl operator (or displacement operator) $D(\boldsymbol{\xi}) = \exp(i\boldsymbol{\xi}^T \Omega \boldsymbol{\chi})$. The phase-space description of Gaussian states is conveniently expressed in terms of the Weyl operators as follows. The Gaussian nature of the quantum state implies that its characteristic function, $\chi_\rho(\boldsymbol{\xi}) = \text{Tr}[\rho D(\boldsymbol{\xi})]$, takes a quadratic exponential form. The Wigner function $W_\rho(\boldsymbol{r})$ is the symplectic Fourier transform of the characteristic function, which—up to normalization—represents the distribution of a photonic quantum state in phase space [86]. For a Gaussian state characterized by a mean vector $\boldsymbol{\mu}$ and a covariance matrix Σ , the Wigner function is proportional to the displaced multivariate Gaussian distribution [38] and has the form

$$W_\rho(\boldsymbol{r}) = \frac{2^d}{\pi^d \sqrt{\det \Sigma}} e^{-(\boldsymbol{r} - \boldsymbol{\mu})^T \Sigma^{-1} (\boldsymbol{r} - \boldsymbol{\mu})}, \quad (23)$$

where $\boldsymbol{r} \in \mathbb{R}^{2d}$ represents the phase-space coordinates. Hence, as expected, the mean vector $\boldsymbol{\mu}$ represents the displacement of the Gaussian state in the phase space and Σ its covariance. This representation highlights that Gaussian states are the “most classical” of quantum states

in the sense that their Wigner functions are non-negative, allowing them to be interpreted as valid probability distributions over phase space.

We call Gaussian transformations those unitary operations that preserve the Gaussian character of photonic quantum states. Equivalently, in the Heisenberg picture, they act on the vector of canonical ladder (or quadrature) operators as symplectic affine transformations. More concretely, the Heisenberg action of the unitary U is given by

$$U^\dagger \boldsymbol{\chi} U = S \boldsymbol{\chi} + \mathbf{r} \mathbb{1}, \quad (24)$$

where S is a real symplectic matrix describing the interferometer and squeezing operations, and $\mathbf{r} \in \mathbb{R}^{2d}$ is a displacement vector. The symplectic matrix S satisfies the constraint

$$S \Omega S^T = \Omega, \quad (25)$$

ensuring the preservation of the canonical commutation relations from Equation (20). As a direct consequence, Gaussian states are closed under such transformations, and their evolution is completely characterized at the level of first and second moments. Hence, the transformation of a mean vector $\boldsymbol{\mu}$ and a covariance matrix Σ under a Gaussian transformation U reads

$$\boldsymbol{\mu} \mapsto S \boldsymbol{\mu} + \mathbf{r}, \quad (26a)$$

$$\Sigma \mapsto S \Sigma S^T. \quad (26b)$$

B Photonic MMD² loss from operator string expectation values

This Appendix contains a derivation of the expression for the squared maximum mean discrepancy (MMD²) loss in the photonic setting in terms of expectation values of operator strings. The resulting form is the bosonic analog of the qubit Pauli- Z string representation from Ref. [23], and parallels the fermionic translation from Ref. [27]. Although this thought carries out verbatim by replacing the Pauli- Z operator to its bosonic analog in the derivation of Ref. [23] for qubit-based systems, we include a self-contained adaptation for completeness.

We consider a binary projective measurement on each mode j , with local projectors $M_0^{(j)}$ and $M_1^{(j)}$, and denote the corresponding global projectors by

$$M_{\mathbf{x}} := \bigotimes_{j=1}^d M_{x_j}^{(j)}, \quad \mathbf{x} \in \{0, 1\}^d. \quad (27)$$

For every subset $A \subseteq [d]$, we define the associated operator string

$$O_A := \sum_{\mathbf{x} \in \{0,1\}^d} (-1)^{|\mathbf{x}_A|} M_{\mathbf{x}} = \bigotimes_{j \in A} (M_0^{(j)} - M_1^{(j)}) \otimes \mathbb{1}_{[d] \setminus A}, \quad (28)$$

where \mathbf{x}_A denotes the restriction of \mathbf{x} to the indices in A , and $|\mathbf{x}_A|$ is its Hamming weight.

Let p and q be two probability distributions on $\{0,1\}^d$. The squared maximum mean discrepancy MMD^2 between them is

$$\text{MMD}^2(p, q) := \mathbb{E}_{\mathbf{x}, \mathbf{x}' \sim p}[K(\mathbf{x}, \mathbf{x}')] + \mathbb{E}_{\mathbf{y}, \mathbf{y}' \sim q}[K(\mathbf{y}, \mathbf{y}')] - 2\mathbb{E}_{\mathbf{x} \sim p, \mathbf{y} \sim q}[K(\mathbf{x}, \mathbf{y})], \quad (29)$$

For the Gaussian kernel

$$K_\sigma(\mathbf{x}, \mathbf{y}) = \exp\left(-\frac{\|\mathbf{x} - \mathbf{y}\|_2^2}{2\sigma}\right) = \prod_{i=1}^d \exp\left(-\frac{(x_i - y_i)^2}{2\sigma}\right), \quad (30)$$

let us define

$$p_\sigma := \frac{1}{2} (1 - e^{-1/(2\sigma)}). \quad (31)$$

Then one readily verifies that

$$\exp\left(-\frac{(x_i - y_i)^2}{2\sigma}\right) = (1 - p_\sigma) + p_\sigma (-1)^{x_i + y_i}. \quad (32)$$

Substituting this identity into the product form of the kernel yields the subset expansion

$$K_\sigma(\mathbf{x}, \mathbf{y}) = \sum_{A \subseteq [d]} p_{K_\sigma}(A) (-1)^{|\mathbf{x}_A|} (-1)^{|\mathbf{y}_A|}, \quad (33)$$

where

$$p_{K_\sigma}(A) := (1 - p_\sigma)^{d-|A|} p_\sigma^{|A|}. \quad (34)$$

Since $\sum_{A \subseteq [d]} p_{K_\sigma}(A) = 1$, this defines a probability distribution over subsets of $[d]$. It is therefore natural to introduce the following:

$$\hat{p}(A) := \sum_{\mathbf{x} \in \{0,1\}^d} p(\mathbf{x}) (-1)^{|\mathbf{x}_A|}, \quad \hat{q}(A) := \sum_{\mathbf{y} \in \{0,1\}^d} q(\mathbf{y}) (-1)^{|\mathbf{y}_A|}. \quad (35)$$

Using Equation (33), we obtain

$$\mathbb{E}_{\mathbf{x} \sim p, \mathbf{y} \sim q}[K_\sigma(\mathbf{x}, \mathbf{y})] = \sum_{A \subseteq [d]} p_{K_\sigma}(A) \hat{p}(A) \hat{q}(A). \quad (36)$$

Applying the same identity to all three terms in the definition of MMD^2 , we arrive at

$$\text{MMD}^2(p, q) = \sum_{A \subseteq [d]} p_{K_\sigma}(A) (\hat{p}(A) - \hat{q}(A))^2 = \mathbb{E}_{A \sim p_{K_\sigma}} \left[(\hat{p}(A) - \hat{q}(A))^2 \right]. \quad (37)$$

Now let ρ_p and ρ_q be quantum states that reproduce the distributions p and q using the binary projective measurement $\{M_{\mathbf{x}}\}_{\mathbf{x} \in \{0,1\}^d}$, i.e.,

$$\text{Tr}[\rho_p M_{\mathbf{x}}] = p(\mathbf{x}), \quad \text{Tr}[\rho_q M_{\mathbf{x}}] = q(\mathbf{x}). \quad (38)$$

Then, by the definition of O_A , we can write that

$$\mathrm{Tr}[\rho_p O_A] = \sum_{\mathbf{x} \in \{0,1\}^d} (-1)^{|\mathbf{x}_A|} p(\mathbf{x}) = \widehat{p}(A), \quad (39)$$

and similarly

$$\mathrm{Tr}[\rho_q O_A] = \sum_{\mathbf{x} \in \{0,1\}^d} (-1)^{|\mathbf{x}_A|} q(\mathbf{x}) = \widehat{q}(A). \quad (40)$$

Hence, the MMD² loss can be written as

$$\mathcal{L}_{\mathrm{MMD}^2}(p, q) = \mathbb{E}_{A \sim p_{K\sigma}} \left[(\langle O_A \rangle_{\rho_p} - \langle O_A \rangle_{\rho_q})^2 \right]. \quad (41)$$

C Parity operator expectation values of Gaussian states

In this Appendix, we derive the exact formula for the parity operator expectation values for Gaussian states for completeness. The expectation value of the parity operator strings correspond to the central values of the Wigner function [87], a well-known fact used extensively in Wigner tomography [60, 61].

Let us start by computing the characteristic function of the single-mode parity operator $(-1)^{\hat{n}}$:

$$\chi_{(-1)^{\hat{n}}}(x, p) := \mathrm{Tr}[PD(x, p)] = e^{-\frac{x^2+p^2}{2}} \sum_{n=0}^{\infty} (-1)^n L_n(x^2 + p^2) = \frac{1}{2}, \quad (42)$$

where $D(x, p)$ denotes the single-mode displacement operator, L_n denotes the Laguerre polynomial of degree n and we have used the well-known identity

$$\sum_{n=0}^{\infty} (-1)^n L_n(x^2 + p^2) = \frac{1}{2} e^{\frac{x^2+p^2}{2}}. \quad (43)$$

Now, consider the global parity operator $\Pi = (-1)^{\hat{n}_1 + \dots + \hat{n}_d}$ defined on a system with d modes. The characteristic function of this operator is simply just

$$\chi_{\Pi}(\boldsymbol{\xi}) = \mathrm{Tr}[\Pi D(\boldsymbol{\xi})] = \frac{1}{2^d}, \quad (44)$$

where $D(\boldsymbol{\xi})$ denotes the multimode displacement operator. Now consider a d -mode photonic quantum state ρ . Its parity expectation value is

$$\mathrm{Tr}[\Pi \rho] = \frac{1}{\pi^d} \int_{\mathbb{C}^d} \chi_{\rho}(\boldsymbol{\xi}) \mathrm{Tr}[\Pi D(-\boldsymbol{\xi})] d^{2d} \boldsymbol{\xi} = \frac{1}{(2\pi)^d} \int_{\mathbb{C}^d} \chi_{\rho}(\boldsymbol{\xi}) d^{2d} \boldsymbol{\xi} = \left(\frac{\pi}{2}\right)^d W_{\rho}(0). \quad (45)$$

Moreover, if ρ is also a Gaussian state and is parametrized by the mean vector $\boldsymbol{\mu}$ and covariance matrix Σ , we can write

$$\text{Tr}[\Pi\rho] = \left(\frac{\pi}{2}\right)^d W_\rho(\mathbf{0}) = \frac{\exp(-\boldsymbol{\mu}^T \Sigma^{-1} \boldsymbol{\mu})}{\sqrt{\det \Sigma}}. \quad (46)$$

Geometrically, the expectation value of the parity operator is proportional to the value of the Wigner function in the center. We note that the expectation value of a parity string corresponding to a subsystem labeled by $A = \{i_1, \dots, i_\ell\}$ is just the expected parity of the state reduced to that subsystem. More concretely, writing

$$\Pi_A := (-1)^{\hat{n}_{i_1} + \dots + \hat{n}_{i_\ell}}, \quad (47)$$

we get that

$$\text{Tr}[\Pi_A \rho] = \text{Tr}[\Pi \text{Tr}_{[n] \setminus A}(\rho)] = \frac{\exp(-\boldsymbol{\mu}_A^T \Sigma_A^{-1} \boldsymbol{\mu}_A)}{\sqrt{\det \Sigma_A}}, \quad (48)$$

where $\boldsymbol{\mu}_A$ and Σ_A are the mean vector and covariance matrix corresponding to $\text{Tr}_{[n] \setminus A}[\rho]$, obtained by removing the rows (and columns) corresponding to $[n] \setminus A$.

Of course, calculating the expected parity of an arbitrary Gaussian state is tractable on a classical computer, but we would like to provide the best possible algorithm in order to push the limits of our proposed algorithm. In our implementation, the time complexity of calculating the parity of a d -mode Gaussian state is $\mathcal{O}(d^3)$, dominated by the Cholesky factorization of the covariance matrix, which involves roughly $d^3/3$ FLOPs. From the Cholesky factor, one can easily obtain both the determinant of Σ and the exponent $\boldsymbol{\mu}^T \Sigma^{-1} \boldsymbol{\mu}$.

D Classical simulation of parity Gaussian Boson Sampling

In this Appendix, we derive a closed expression for parity-outcome probabilities of general Gaussian states and analyze their classical evaluation. We show how parity-string expectation values can be precomputed and reused in a mode-by-mode sampling scheme, discuss the resulting computational scaling, and identify lossy regimes where parity-based sampling may become competitive with existing classical simulation methods.

Detecting parity \boldsymbol{x} in a Gaussian state ρ characterized by a mean vector $\boldsymbol{\mu}$ and a covariance matrix Σ has probability

$$\begin{aligned} p(\boldsymbol{x}) &= \text{Tr} \left[\rho \bigotimes_{i=1}^d \left(\frac{1 + (-1)^{x_i} (-1)^{\hat{n}_i}}{2} \right) \right] = \frac{1}{2^d} \sum_{S \subseteq [d]} (-1)^{|\boldsymbol{x}_S|} \text{Tr} [\Pi_S \rho] \\ &= \frac{1}{2^d} \sum_{S \subseteq [d]} (-1)^{|\boldsymbol{x}_S|} \frac{\exp(-\boldsymbol{\mu}_S^T \Sigma_S^{-1} \boldsymbol{\mu}_S)}{\sqrt{\det \Sigma_S}}. \end{aligned} \quad (49)$$

As the same parities can be reused during the mode-by-mode sampling algorithm, it is best to have all the parities calculated in advance for all the 2^d possible subsystems, which naively requires at most $\mathcal{O}(d^3 2^d)$ resources. However, due to the data dependency of the Cholesky factorization detailed in Ref. [88], the algorithm does not need to redo the full Cholesky factorization from scratch for every summand. With this strategy, we expect a significant polynomial improvement in the time complexity. Moreover, we can reuse the previously calculated probability during mode-by-mode sampling using

$$p(x_n, x_{n-1}, \dots, x_1) = p(x_{n-1}, \dots, x_1) - \frac{1}{2^{n-1}} \sum_{S \subseteq [n-1]} (-1)^{|\mathbf{x}_S|} \text{Tr} [\Pi_{S \cup \{n\}} \rho]. \quad (50)$$

However, we note that for simulating ideal Gaussian Boson Sampling, combining coarse-graining with current state-of-the-art classical simulation algorithms for particle-number resolved detection, such as the approach presented in Ref. [48] with cost scaling as $\tilde{\mathcal{O}}(2^{d/2})$ in the worst case, are more efficient than using Equation (49) directly.

Notably, the last expression is similar to the loop torontonian ltor introduced in Ref. [46]. In fact, one can rewrite Equation (49) for the special case of $\mathbf{x} = \mathbf{1} := [1, \dots, 1]^T$ as

$$p(\mathbf{1}) = \frac{(-1)^d e^{-\boldsymbol{\mu}^T \Sigma^{-1} \boldsymbol{\mu}}}{2^d \sqrt{\det \Sigma}} \text{ltor}(\mathbb{1} - \Sigma^{-1}, \sqrt{2} \Sigma^{-1} \boldsymbol{\mu}). \quad (51)$$

However, as opposed to the threshold detection probabilities, parity-outcome probabilities can be written as an expectation value of parity expectation values that are in the interval $[-1, 1]$. Hence, one can utilize a simple Hoeffding's inequality to get an additive error approximation of this probability, yielding an approximate classical sampling strategy. This can be beneficial in the setting where the Gaussian Boson Sampling experiment is lossy, as higher-order parity-string expectation values are suppressed by losses, an observation already used for devising a classical simulation algorithm for lossy Gaussian Boson Sampling in Ref. [50].

Moreover, as expected from the discussion in Appendix B, we can rewrite the probabilities from Equation (49) as the Walsh-Hadamard transform of the parity expectation values as

$$p(\mathbf{x}) := \frac{1}{2^d} \sum_{\mathbf{s} \in \{0,1\}^d} (-1)^{\mathbf{x} \cdot \mathbf{s}} \langle \Pi_{\xi(\mathbf{s})} \rangle_\rho, \quad (52)$$

where $\xi(\mathbf{s}) := \{s_i \in [d] : s_i = 1\}$. Hence, given all the parity expectation values for all 2^d subsystems, one can compute the parity detection probabilities in $\mathcal{O}(d 2^d)$ time using the fast Walsh-Hadamard transform [89].

E Classical training of threshold GBBMs

This Appendix outlines the classical simulation algorithm for training threshold GBBMs. Transitioning from parity GBBMs to threshold GBBMs requires replacing parity operator strings

with threshold operator strings, a shift that necessitates a fundamentally different set of formulas for the classical training procedure.

We construct a generic threshold operator string for a subset of modes $A \subseteq [d]$ as follows:

$$T_A = \bigotimes_{j \in A} (2 |0_j\rangle\langle 0_j| - \mathbb{1}_j) \otimes \mathbb{1}_{[d] \setminus A}. \quad (53)$$

To compute the expectation value of T_A by a Gaussian state ρ , we apply an inclusion-exclusion expansion over the subsets $S \subseteq A$:

$$\langle T_A \rangle_\rho = (-1)^{|A|} \sum_{S \subseteq A} (-2)^{|S|} p_0(S). \quad (54)$$

In this expression, $p_0(S)$ denotes the probability of detecting the Gaussian state ρ as a vacuum on modes labeled by S . This can be computed using the overlap formula [38] as

$$p_0(S) = \frac{\exp\left(-\frac{1}{2} \boldsymbol{\mu}_S^\dagger Q_S^{-1} \boldsymbol{\mu}_S\right)}{\sqrt{\det Q_S}}, \quad (55)$$

where $\boldsymbol{\mu}_S$ and Q_S denote the mean vector and Husimi covariance matrix of the original Gaussian state restricted to modes defined by S . The full Husimi matrix is related to the covariance matrix as $Q = \frac{1}{2}(\Sigma + \mathbb{1})$.

With the analytical form of the expectation value established, we can now assess the computational complexity of evaluating these formulas during training. The primary bottleneck lies in the inclusion-exclusion expansion, which requires computing the vacuum detection probabilities for all $2^{|A|}$ subsets. Since evaluating each overlap involves the determinant and inverse of a matrix up to size $|A| \times |A|$, we arrive at the following result regarding the scalability of the threshold GBBMs:

Theorem 2 (Classical trainability of threshold GBBMs). For a GBBM over d bosonic modes, as defined in Definition 1, the expectation value of any length- ℓ threshold string can be evaluated classically in $\mathcal{O}(\ell^3 2^\ell)$ time, given the corresponding covariance matrix. This covariance matrix can be computed in $\mathcal{O}(Ld^3)$ time using $\mathcal{O}(d^2)$ memory. Consequently, the model admits efficient classical training via automatic differentiation and backpropagation, when threshold operator strings are of length $\mathcal{O}(\log(d))$.

Proof. The evaluation of the covariance matrix is exactly the same as in Theorem 1. Moreover, evaluating Equation (54) requires $\mathcal{O}(\ell^3 2^\ell)$ steps, as the algorithm needs to iterate over 2^ℓ summands, and each summand requires computing a determinant and an inverse (or solving the equivalent linear system) which requires $\mathcal{O}(\ell^3)$ time to evaluate. Consequently, the model admits efficient classical training for threshold operator strings that are of length $\ell = \mathcal{O}(\log(d))$, as this yields an evaluation time for the threshold operator string expectation values of $\mathcal{O}(\text{poly}(d))$. \square

While the results in Section 4.5 indicate that the threshold-based approach maintains robustness in regimes where parity-based methods fail to converge, this performance comes at the cost of classical training efficiency. This highlights a fundamental trade-off between the expressivity of the model and its computational overhead during classical training.

Notably, the parity-based and threshold-based variants converge in the dilute regime, where the number of modes scales at least quadratically with the total photon count ($n = \mathcal{O}(\sqrt{d})$). Given that parity-based GBBMs offer superior classical training efficiency, they can serve as an effective pre-training stage for threshold models. This hierarchical approach significantly reduces the overall computational overhead of training the more expressive threshold-based variant.

F Training set visualization

Here we present a few examples of the cellular automaton and binarized USPS datasets, naturally defined over 6×18 and 16×16 grids, respectively. Random samples are shown in Fig. 6.

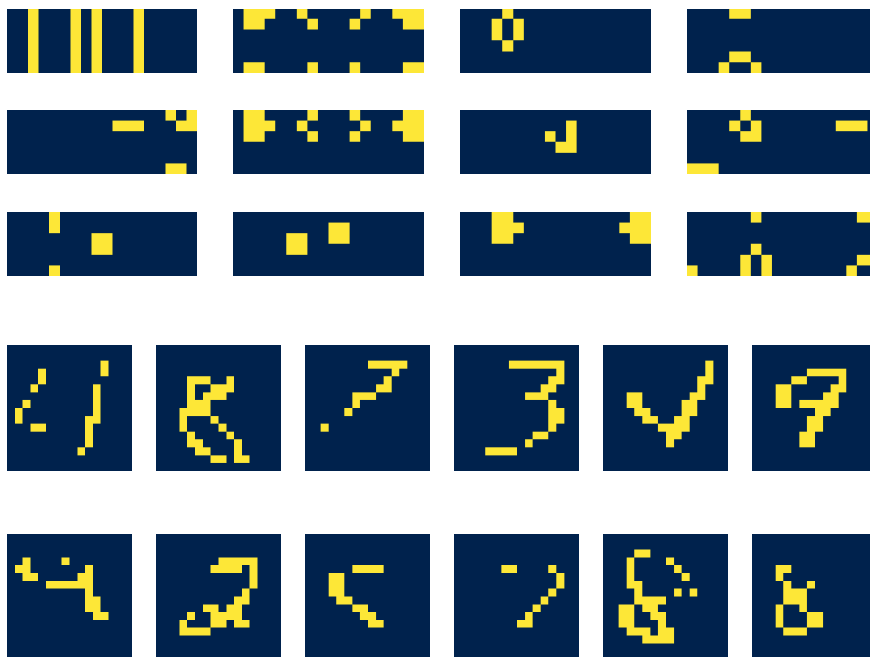


Figure 6: Examples from the cellular automaton (top) and USPS (bottom) training datasets.

References

- [1] I. Goodfellow, Y. Bengio, and A. Courville. *Deep Learning*. <http://www.deeplearningbook.org>. MIT Press, 2016.
- [2] A. G. Baydin, B. A. Pearlmutter, A. A. Radul, and J. M. Siskind. “Automatic differentiation in machine learning: a survey”. *J. Mach. Learn. Res.* 18 (2018), pp. 1–43. DOI: 10.5555/3122009.3242010.
- [3] Y. Bengio, E. Laufer, G. Alain, and J. Yosinski. “Deep generative stochastic networks trainable by backprop”. *International conference on machine learning*. PMLR. 2014, pp. 226–234. DOI: 10.5555/3044805.3044918.
- [4] E. R. Anschuetz and B. T. Kiani. “Quantum variational algorithms are swamped with traps”. *Nat. Commun.* 13 (2022), p. 7760. DOI: 10.1038/s41467-022-35364-5.
- [5] J. R. McClean, S. Boixo, V. N. Smelyanskiy, R. Babbush, and H. Neven. “Barren plateaus in quantum neural network training landscapes”. *Nat. Commun.* 9 (2018), p. 4812. DOI: 10.1038/s41467-018-07090-4.
- [6] M. Larocca, S. Thanasilp, S. Wang, K. Sharma, J. Biamonte, P. J. Coles, L. Cincio, J. R. McClean, Z. Holmes, and M. Cerezo. “Barren plateaus in variational quantum computing”. *Nat. Rev. Phys.* (2025), pp. 1–16. DOI: 10.1038/s42254-025-00813-9.
- [7] A. Abbas, R. King, H.-Y. Huang, W. J. Huggins, R. Movassagh, D. Gilboa, and J. R. McClean. “On quantum backpropagation, information reuse, and cheating measurement collapse”. *Proceedings of the 37th International Conference on Neural Information Processing Systems*. NIPS ’23. New Orleans, LA, USA: Curran Associates Inc., 2023. URL: <https://dl.acm.org/doi/10.5555/3666122.3668062>.
- [8] A. Gilyén, S. Arunachalam, and N. Wiebe. “Optimizing quantum optimization algorithms via faster quantum gradient computation”. *Proceedings of the Thirtieth Annual ACM-SIAM Symposium on Discrete Algorithms*. SIAM. 2019, pp. 1425–1444. DOI: 10.1137/1.9781611975482.87.
- [9] T. Hoeffler, T. Haener, and M. Troyer. *Disentangling Hype from Practicality: On Realistically Achieving Quantum Advantage*. 2023. arXiv: 2307.00523 [quant-ph].
- [10] K. Mitarai, M. Negoro, M. Kitagawa, and K. Fujii. “Quantum circuit learning”. *Phys. Rev. A* 98 (2018). DOI: 10.1103/physreva.98.032309.
- [11] M. Schuld, V. Bergholm, C. Gogolin, J. Izaac, and N. Killoran. “Evaluating analytic gradients on quantum hardware”. *Phys. Rev. A* 99 (2019). DOI: 10.1103/physreva.99.032331.
- [12] D. Wierichs, J. Izaac, C. Wang, and C. Y.-Y. Lin. “General parameter-shift rules for quantum gradients”. *Quantum* 6 (2022), p. 677. DOI: 10.22331/q-2022-03-30-677.

- [13] A. Pappalardo, P.-E. Emeriau, G. de Felice, B. Ventura, H. Jaunin, R. Yeung, B. Coecke, and S. Mansfield. “Photonic parameter-shift rule: Enabling gradient computation for photonic quantum computers”. *Physical Review A* 111 (2025). DOI: 10.1103/physreva.111.032429.
- [14] R. Sweke, F. Wilde, J. Meyer, M. Schuld, P. K. Faehrmann, B. Meynard-Piganeau, and J. Eisert. “Stochastic gradient descent for hybrid quantum-classical optimization”. *Quantum* 4 (2020), p. 314. DOI: 10.22331/q-2020-08-31-314.
- [15] B. Coyle, S. Raj, N. Mathur, E. A. Cherrat, N. Jain, S. Kazdaghli, and I. Kerenidis. “Training-efficient density quantum machine learning”. *npj Quantum Information* 11 (2025), p. 172. DOI: 10.1038/s41534-025-01099-6.
- [16] J. Bowles, D. Wierichs, and C.-Y. Park. “Backpropagation scaling in parameterised quantum circuits”. *Quantum* 9 (2025), p. 1873. DOI: 10.22331/q-2025-10-02-1873.
- [17] Q. T. Nguyen, L. Schatzki, P. Braccia, M. Ragone, P. J. Coles, F. Sauvage, M. Larocca, and M. Cerezo. “Theory for Equivariant Quantum Neural Networks”. *PRX Quantum* 5 (2024), p. 020328. DOI: 10.1103/PRXQuantum.5.020328.
- [18] L. Monbroussou, E. Z. Mamon, J. Landman, A. B. Grilo, R. Kukla, and E. Kashefi. “Trainability and Expressivity of Hamming-Weight Preserving Quantum Circuits for Machine Learning”. *Quantum* 9 (2025), p. 1745. DOI: 10.22331/q-2025-05-15-1745.
- [19] M. Larocca, F. Sauvage, F. M. Sbahi, G. Verdon, P. J. Coles, and M. Cerezo. “Group-Invariant Quantum Machine Learning”. *PRX Quantum* 3 (2022), p. 030341. DOI: 10.1103/PRXQuantum.3.030341.
- [20] J. J. Meyer, M. Mularski, E. Gil-Fuster, A. A. Mele, F. Arzani, A. Wilms, and J. Eisert. “Exploiting Symmetry in Variational Quantum Machine Learning”. *PRX Quantum* 4 (2023), p. 010328. DOI: 10.1103/PRXQuantum.4.010328.
- [21] H. Zheng, Z. Li, J. Liu, S. Strelchuk, and R. Kondor. “Speeding Up Learning Quantum States Through Group Equivariant Convolutional Quantum Ansätze”. *PRX Quantum* 4 (2023), p. 020327. DOI: 10.1103/PRXQuantum.4.020327.
- [22] S. Kasture, O. Kyriienko, and V. E. Elfving. “Protocols for classically training quantum generative models on probability distributions”. *Phys. Rev. A* 108 (2023). DOI: 10.1103/physreva.108.042406.
- [23] M. S. Rudolph, S. Lerch, S. Thanasilp, O. Kiss, O. Shaya, S. Vallecorsa, M. Grossi, and Z. Holmes. “Trainability barriers and opportunities in quantum generative modeling”. *npj Quantum Inf.* 10 (2024). DOI: 10.1038/s41534-024-00902-0.
- [24] E. Recio-Armengol and J. Bowles. *IQPopt: Fast optimization of instantaneous quantum polynomial circuits in JAX*. 2025. arXiv: 2501.04776 [quant-ph].

- [25] E. Recio-Armengol, S. Ahmed, and J. Bowles. *Train on classical, deploy on quantum: scaling generative quantum machine learning to a thousand qubits*. 2025. arXiv: 2503.02934 [quant-ph].
- [26] A. Kurkin, K. Shen, S. Pielawa, H. Wang, and V. Dunjko. *Universality and kernel-adaptive training for classically trained, quantum-deployed generative models*. 2025. arXiv: 2510.08476 [quant-ph].
- [27] B. Bakó, Z. Kolarovszki, and Z. Zimborás. *Fermionic Born Machines: Classical training of quantum generative models based on Fermion Sampling*. 2025. arXiv: 2511.13844 [quant-ph].
- [28] M. Oszmaniec, N. Dangniam, M. E. Morales, and Z. Zimborás. “Fermion Sampling: A Robust Quantum Computational Advantage Scheme Using Fermionic Linear Optics and Magic Input States”. *PRX Quantum* 3 (2022). DOI: 10.1103/prxquantum.3.020328.
- [29] C. S. Hamilton, R. Kruse, L. Sansoni, S. Barkhofen, C. Silberhorn, and I. Jex. “Gaussian Boson Sampling”. *Phys. Rev. Lett.* 119 (2017), p. 170501. DOI: 10.1103/PhysRevLett.119.170501.
- [30] R. Kruse, C. S. Hamilton, L. Sansoni, S. Barkhofen, C. Silberhorn, and I. Jex. “Detailed study of Gaussian boson sampling”. *Phys. Rev. A* 100 (2019), p. 032326. DOI: 10.1103/PhysRevA.100.032326.
- [31] B. Go, C. Oh, and H. Jeong. *Sufficient conditions for hardness of lossy Gaussian boson sampling*. 2025. arXiv: 2511.07853 [quant-ph].
- [32] Z. Li, N. R. Solomons, J. F. F. Bulmer, R. B. Patel, and I. A. Walmsley. “A complexity transition in displaced Gaussian Boson Sampling”. *npj Quantum Information* 11 (2025), p. 119. DOI: 10.1038/s41534-025-01062-5.
- [33] D. Cogan, Z.-E. Su, O. Kenneth, and D. Gershoni. *A deterministic source of indistinguishable photons in a cluster state*. 2021. arXiv: 2110.05908 [quant-ph].
- [34] H.-L. Liu et al. *Robust quantum computational advantage with programmable 3050-photon Gaussian boson sampling*. 2025. arXiv: 2508.09092 [quant-ph].
- [35] F. Arute et al. “Quantum supremacy using a programmable superconducting processor”. *Nature* 574 (2019), pp. 505–510. DOI: 10.1038/s41586-019-1666-5.
- [36] R. Acharya et al. “Suppressing quantum errors by scaling a surface code logical qubit”. *Nature* 614 (2023), pp. 676–681. DOI: 10.1038/s41586-022-05434-1.
- [37] P. Stano and D. Loss. “Review of performance metrics of spin qubits in gated semiconducting nanostructures”. *Nat. Rev. Phys.* 4 (2022), pp. 672–688. DOI: 10.1038/s42254-022-00484-w.
- [38] A. Serafini. *Gaussian States of Continuous Variable Systems*. CRC Press, Taylor & Francis Group, 2017.

- [39] G. Adesso, S. Ragy, and A. R. Lee. “Continuous Variable Quantum Information: Gaussian States and Beyond”. *Open Systems & Information Dynamics* 21 (2014), p. 1440001. DOI: 10.1142/s1230161214400010.
- [40] S. Aaronson and A. Arkhipov. “The Computational Complexity of Linear Optics”. *Proceedings of the Forty-Third Annual ACM Symposium on Theory of Computing (STOC '11)*. ACM, 2011, pp. 333–342. DOI: 10.1145/1993636.1993682.
- [41] E. R. Caianiello. *Combinatorics & Renormalization in Quantum Field Theory*. Vol. 38. Reading: Benjamin, 1973. URL: <https://www.osti.gov/biblio/4338754>.
- [42] D. Grier, D. J. Brod, J. M. Arrazola, M. B. d. A. Alonso, and N. Quesada. “The Complexity of Bipartite Gaussian Boson Sampling”. *Quantum* 6 (2022), p. 863. DOI: 10.22331/q-2022-11-28-863.
- [43] H.-S. Zhong, H. Wang, Y.-H. Deng, M.-C. Chen, L.-C. Peng, Y.-H. Luo, J. Qin, D. Wu, X. Ding, Y. Hu, P. Hu, X.-Y. Yang, W.-J. Zhang, H. Li, and Y. Li et al. “Quantum computational advantage using photons”. *Science* 370 (2020), pp. 1460–1463. DOI: 10.1126/science.abe8770.
- [44] H.-S. Zhong et al. “Phase-Programmable Gaussian Boson Sampling Using Stimulated Squeezed Light”. *Phys. Rev. Lett.* 127 (2021). DOI: 10.1103/physrevlett.127.180502.
- [45] L. S. Madsen, F. Laudenbach, M. F. Askarani, F. Rortais, T. Vincent, J. F. F. Bulmer, F. M. Miatto, L. Neuhaus, L. G. Helt, M. J. Collins, A. Lita, T. Gerrits, S. Nam, V. Vaidya, and M. M. et al. “Quantum computational advantage with a programmable photonic processor”. *Nature* 606 (2022), pp. 75–81. DOI: 10.1038/s41586-022-04725-x.
- [46] N. Quesada, J. M. Arrazola, T. Vincent, H. Qi, and R. García-Patrón. *Quadratic speedup for simulating Gaussian boson sampling*. 2021. arXiv: 2010.15595 [quant-ph].
- [47] J. F. F. Bulmer, S. Paesani, R. S. Chadwick, and N. Quesada. “Threshold detection statistics of bosonic states”. *Phys. Rev. A* 106 (2022). DOI: 10.1103/physreva.106.043712.
- [48] J. F. F. Bulmer, B. A. Bell, R. S. Chadwick, A. E. Jones, D. Moise, A. Rigazzi, J. Thorbecke, U.-U. Haus, T. V. Vaerenbergh, R. B. Patel, I. A. Walmsley, and A. Laing. “The boundary for quantum advantage in Gaussian boson sampling”. *Science Advances* 8 (2022). DOI: 10.1126/sciadv.ab19236.
- [49] C. Oh, M. Liu, Y. Alexeev, B. Fefferman, and L. Jiang. “Classical algorithm for simulating experimental Gaussian boson sampling”. *Nature Physics* 20 (2024), pp. 1461–1468. DOI: 10.1038/s41567-024-02535-8.
- [50] T. Dodd, J. Martínez-Cifuentes, O. T. Brown, N. Quesada, and R. García-Patrón. *A fast and frugal Gaussian Boson Sampling emulator*. 2025. arXiv: 2511.14923 [quant-ph].

- [51] M. Benedetti, D. Garcia-Pintos, O. Perdomo, V. Leyton-Ortega, Y. Nam, and A. Perdomo-Ortiz. “A generative modeling approach for benchmarking and training shallow quantum circuits”. *npj Quantum Inf.* 5 (2019), p. 45. DOI: 10.1038/s41534-019-0157-8.
- [52] J.-G. Liu and L. Wang. “Differentiable learning of quantum circuit Born machines”. *Phys. Rev. A* 98 (2018), p. 062324. DOI: 10.1103/PhysRevA.98.062324.
- [53] B. Coyle, D. Mills, V. Danos, and E. Kashefi. “The Born supremacy: quantum advantage and training of an Ising Born machine”. *npj Quantum Inf.* 6 (2020), p. 60. DOI: 10.1038/s41534-020-00288-9.
- [54] A. Salavrakos, T. Sedrakyan, J. Mills, S. Mansfield, and R. Mezher. “Error-mitigated photonic quantum circuit Born machine”. *Physical Review A* 111 (2025). DOI: 10.1103/physreva.111.1030401.
- [55] I. Čepaitė, B. Coyle, and E. Kashefi. “A continuous variable Born machine”. *Quantum Machine Intelligence* 4 (2022). DOI: 10.1007/s42484-022-00063-3.
- [56] Z. Kolarovszki, D. T. R. Nagy, and Z. Zimborás. “On the Learning Abilities of Photonic Continuous-Variable Born Machines”. *IEEE Quantum Week, QCE 2024 Proceedings*. Vol. 01. 2024, pp. 750–756. DOI: 10.1109/QCE60285.2024.00094.
- [57] A. Gretton, K. M. Borgwardt, M. J. Rasch, B. Schölkopf, and A. Smola. “A Kernel Two-Sample Test”. *Journal of Machine Learning Research* 13 (2012), pp. 723–773. URL: <http://jmlr.org/papers/v13/gretton12a.html>.
- [58] C. C. Gerry and J. Mimih. “The parity operator in quantum optical metrology”. *Contemporary Physics* 51 (2010), pp. 497–511. DOI: 10.1080/00107514.2010.509995.
- [59] N. Quesada, J. M. Arrazola, and N. Killoran. “Gaussian boson sampling using threshold detectors”. *Phys. Rev. A* 98 (2018), p. 062322. DOI: 10.1103/PhysRevA.98.062322.
- [60] M. Hofheinz, H. Wang, M. Ansmann, R. C. Bialczak, E. Lucero, M. Neeley, A. O’connell, D. Sank, J. Wenner, J. M. Martinis, et al. “Synthesizing arbitrary quantum states in a superconducting resonator”. *Nature* 459 (2009), pp. 546–549.
- [61] B. Vlastakis, G. Kirchmair, Z. Leghtas, S. E. Nigg, L. Frunzio, S. M. Girvin, M. Mirrahimi, M. H. Devoret, and R. J. Schoelkopf. “Deterministically encoding quantum information using 100-photon Schrödinger cat states”. *Science* 342 (2013), pp. 607–610.
- [62] R. H. Hadfield. “Single-photon detectors for optical quantum information applications”. *Nature Photonics* 3 (2009), pp. 696–705. DOI: 10.1038/nphoton.2009.230.
- [63] N. Killoran, T. R. Bromley, J. M. Arrazola, M. Schuld, N. Quesada, and S. Lloyd. “Continuous-variable quantum neural networks”. *Phys. Rev. Res.* 1 (2019), p. 033063. DOI: 10.1103/PhysRevResearch.1.033063.
- [64] W. R. Clements, P. C. Humphreys, B. J. Metcalf, W. S. Kolthammer, and I. A. Walmsley. “Optimal design for universal multiport interferometers”. *Optica* 3 (2016), pp. 1460–1465. DOI: 10.1364/OPTICA.3.001460.

- [65] M. Reck, A. Zeilinger, H. J. Bernstein, and P. Bertani. “Experimental realization of any discrete unitary operator”. *Phys. Rev. Lett.* 73 (1994), pp. 58–61. DOI: 10.1103/PhysRevLett.73.58.
- [66] G. Cariolaro and G. Pierobon. “Bloch-Messiah reduction of Gaussian unitaries by Takagi factorization”. *Phys. Rev. A* 94 (2016), p. 062109.
- [67] A. Bouland, D. Brod, I. Datta, B. Fefferman, D. Grier, F. Hernandez, and M. Oszmaniec. *Complexity-theoretic foundations of BosonSampling with a linear number of modes*. 2025. arXiv: 2312.00286 [quant-ph].
- [68] *Source code for the classical training of GBBMs*. URL: https://github.com/Budapest-Quantum-Computing-Group/gaussian_bosonic_born_machines (last accessed on 03/11/2026).
- [69] J. Bradbury, R. Frostig, P. Hawkins, M. J. Johnson, C. Leary, D. Maclaurin, G. Necula, A. Paszke, J. VanderPlas, S. Wanderman-Milne, and Q. Zhang. *JAX: composable transformations of Python+NumPy programs*. Version 0.3.13. 2018. URL: <http://github.com/google/jax> (last accessed on 05/17/2025).
- [70] D. Garreau, W. Jitkrittum, and M. Kanagawa. *Large sample analysis of the median heuristic*. 2018. arXiv: 1707.07269 [math.ST].
- [71] D. Kingma and J. Ba. “Adam: A Method for Stochastic Optimization”. *International Conference on Learning Representations (ICLR)*. San Diego, CA, USA, 2015. URL: <https://inspirehep.net/literature/1670744>.
- [72] D. H. Ackley, G. E. Hinton, and T. J. Sejnowski. “A learning algorithm for boltzmann machines”. *Cognitive Science* 9 (1985), pp. 147–169. DOI: 10.1016/S0364-0213(85)80012-4.
- [73] K. P. Murphy. *Machine learning: a probabilistic perspective*. MIT press, 2012. URL: <https://dl.acm.org/doi/book/10.5555/2380985>.
- [74] F. Pedregosa, G. Varoquaux, A. Gramfort, V. Michel, B. Thirion, O. Grisel, M. Blondel, P. Prettenhofer, R. Weiss, V. Dubourg, J. Vanderplas, A. Passos, D. Cournapeau, M. Brucher, M. Perrot, and E. Duchesnay. “Scikit-learn: Machine Learning in Python”. *Journal of Machine Learning Research* 12 (2011), pp. 2825–2830. URL: <https://jmlr.org/papers/v12/pedregosa11a.html>.
- [75] *Benchmarking for quantum machine learning models*. URL: <https://github.com/XanaduAI/qml-benchmarks> (last accessed on 11/16/2025).
- [76] C. Chow and C. Liu. “Approximating discrete probability distributions with dependence trees”. *IEEE Trans. Inf. Theory* 14 (1968), pp. 462–467. DOI: 10.1109/TIT.1968.1054142.
- [77] A. Ankan and J. Textor. “pgmpy: A Python Toolkit for Bayesian Networks”. *J. Mach. Learn. Res.* 25 (2024), pp. 1–8. URL: <http://jmlr.org/papers/v25/23-0487.html>.

- [78] A. Adamatzky. *Game of life cellular automata*. Vol. 1. Springer, 2010. DOI: 10.1007/978-1-84996-217-9.
- [79] B. Bakó, D. T. R. Nagy, P. Hága, Z. Kallus, and Z. Zimborás. *Problem-informed Graphical Quantum Generative Learning*. 2025. arXiv: 2405.14072 [quant-ph].
- [80] J. J. Hull. “A database for handwritten text recognition research”. *IEEE Transactions on Pattern Analysis and Machine Intelligence* 16 (1994), pp. 550–554. DOI: 10.1109/34.291440.
- [81] J. Bowles. *Genomic*. <https://pennylane.ai/datasets/other/genomic>. 2025.
- [82] B. Yelmen, A. Decelle, L. Ongaro, D. Marnetto, C. Tallec, F. Montinaro, C. Furtlehner, L. Pagani, and F. Jay. “Creating artificial human genomes using generative neural networks”. *PLoS genetics* 17 (2021), e1009303.
- [83] A. Morningstar and R. G. Melko. “Deep learning the ising model near criticality”. *Journal of Machine Learning Research* 18 (2018), pp. 1–17.
- [84] A. Kurkin, U. Chabaud, Z. Kolarovszki, B. Bakó, Z. Zimborás, and V. Dunjko. “Universality of Classically Trainable, Quantum-Deployed Boson-Sampling Generative Models” (2026).
- [85] F. Gottlieb, R. Mezher, B. Ventura, S. Mansfield, and A. Salavrakos. “Efficient training of photonic quantum generative models” (2026).
- [86] E. Wigner. “On the Quantum Correction For Thermodynamic Equilibrium”. *Phys. Rev.* 40 (1932), pp. 749–759. DOI: 10.1103/PhysRev.40.749.
- [87] K. E. Cahill and R. J. Glauber. “Density Operators and Quasiprobability Distributions”. *Phys. Rev.* 177 (1969), pp. 1882–1902. DOI: 10.1103/PhysRev.177.1882.
- [88] Á. Kaposi, Z. Kolarovszki, T. Kozsik, Z. Zimborás, and P. Rakyta. *Polynomial speedup in Torontonian calculation by a scalable recursive algorithm*. 2022. arXiv: 2109.04528 [quant-ph].
- [89] Fino and Algazi. “Unified Matrix Treatment of the Fast Walsh-Hadamard Transform”. *IEEE Transactions on Computers* C-25 (1976), pp. 1142–1146. DOI: 10.1109/TC.1976.1674569.